Modeling of aerosol property evolution during winter haze episodes over a megacity cluster in northern China: Roles of regional transport and heterogeneous reactions of SO_2

Huiyun Du[1,2], Jie Li[1,2,3*], Xueshun Chen[1], Zifa Wang[1,2,3], Yele Sun[1,2,3], Pingqing Fu[1], Jianjun Li[4], Jian Gao[5], Ying Wei[1,2]

[1] LAPC, Institute of Atmospheric Physics, Chinese Academy of Sciences, Beijing 100029, China

[2] College of Earth Sciences, University of Chinese Academy of Sciences, Beijing 100029, China

[3] Center for Excellence in Urban Atmospheric Environment, Institute of Urban Environment, Chinese Academy of Sciences, Xiamen, China

[4] China National Environmental Monitoring Center, Beijing, China

[5] Chinese Research Academy of Environmental Sciences

Abstract. Regional transport and heterogeneous reactions played crucial roles in haze formation over a megacity cluster centered on Beijing. In this study, the updated Nested Air Quality Prediction Model System (NAQPMS) and the HYSPLIT Lagrangian trajectory model were employed to investigate the evolution of aerosols—in terms of the number concentration, size distribution, and aging degree—in Beijing during six haze episodes between November 15 and December 15, 2016, as part of the Air Pollution and Human Health–Beijing (APHH-Beijing) winter campaign of 2016. The model exhibited reasonable performance not only in mass concentrations of $PM_{2.5}$ and its components in Beijing but also in the number concentration, size distribution, and aging degree. We revealed that regional transport played a nonnegligible role in haze episodes, with contributions of 14%–31% to the surface $PM_{2.5}$ mass concentration. The contribution of regional transport to secondary inorganic aerosols was larger than that to primary aerosols (30%–63% vs. 3%–12%). The chemical transformation of SO_2 in the transport pathway from source regions to Beijing was the major form of SO_4^{2-} regional transport. We also found that sulfate formed outside Beijing from SO_2 emitted in Beijing; this sulfate was then blown back to Beijing and considerably influenced haze formation. In the transport pathway, aerosols underwent aging, which altered the

mass ratio of coating to black carbon (R_{BC}) and the size distribution of number concentrations. During the episodes, the geometric mean diameter (GMD) increased from less than 100 nm at the initial site to approximately 120 nm at the final site (Beijing), and R_{BC} increased from 2–4 to 4–8. These changes would affect regional radiation and climate. In haze episodes with high humidity, the average contributions of gas and aqueous chemistry, heterogeneous chemistry, and primary emission to sulfate were comparable. Primary emissions had the greatest impact under light to moderate pollution levels, whereas heterogeneous chemistry had a stronger effect under high pollution levels.

Keywords: Regional transport; heterogeneous reactions; number size distribution; NAQPMS

1 Introduction

In past decades, a megacity cluster in China that is centered on Beijing and includes 28 cities (272,500 km^2, a population of 191.7 million people) has been experienced frequent severe and persistent haze episodes (Zhao et al., 2013; Sun et al., 2014; Sun et al., 2016). $PM_{2.5}$ levels exceeding 500 μg m^{-3} have often been reported. The adverse effects of $PM_{2.5}$ on visibility, climate, and particularly human health have drawn widespread public attention (Hyslop, 2009; Chen et al., 2018; Yang et al., 2017a; Yang et al., 2017b; Anderson et al., 2010). Although the $PM_{2.5}$ concentration in Beijing has decreased by 35% in the recent 5 years (2013–2017) benefiting from implementation of the Atmospheric Pollution Prevention and Control Action Plan, the $PM_{2.5}$ level in 2017 still reached 58 μg m^{-3}, which is 1.7 times the World Health Organization-recommended safe level of 35 μg m^{-3} (http://www.bjepb.gov.cn/bjhrb/index/index.html). Understanding the mechanism of haze episodes in this megacity cluster is thus an urgent task for policymakers.

Observations have revealed that haze episodes in this megacity cluster are mainly caused by the rapid formation of secondary inorganic species (SIA, including sulfate, nitrate, and ammonium) (Huang et al., 2014; Zheng et al., 2015; Han et al., 2016). The

SIA mass fraction in $PM_{2.5}$ can be up to 55% on severe pollution days, which is 2.5 times that on clear days (Ma et al., 2017). Tang et al. (2016a) proposed that local chemical transformation associated with humidity dominated the rapid formation of SIA in Beijing. Yang et al. (2015) argued that local chemical conversion would not be fully able to explain the observed rapid formation of SIA in a short time. Using a ceilometer and in situ observation data, Zhu et al. (2016) and Ma et al. (2017) further proposed that regional transport was the major cause of the initial haze stage and that local chemistry, particularly heterogeneous chemistry, dominated the later rise in Beijing. This result is different from the findings of modeling studies (Timmermans et al., 2017; Li and Han, 2016; Li et al.,2017), in which regional transport was identified as the dominant factor during haze episodes in the megacity cluster. Comprehensive observations of the physicochemical properties (e.g., mixing state, number concentration, and size distribution) of aerosols can provide more insights into the accuracy of regional transport and chemistry assessment. Black carbon (BC) is usually more thickly coated by SIA and organic aerosols in transported and aged air masses than in fresh particles, as indicated by higher fractal dimension (Wang et al., 2017b), larger coating fraction (ratio of variation in BC mass equivalent diameter to initial BC diameter, $\Delta D_{me}/D_{me,0}$) (Peng et al., 2016) and the higher mass ratio of coating to BC (R_{BC}) (Wang et al., 2018a). Massoli et al. (2015) and Wang et al. (2017) reported that R_{BC} exceeded 10 in remote sites after BC had undergone long-term transport. This value was much higher than that in an urban area with high fresh particle emissions, where R_{BC} generally was less than 1.5 (Liu et al., 2017). The geometric mean diameter (GMD) of $PM_{2.5}$ also changed significantly due to the impact of regional transport. In haze episodes in Beijing, the GMD increased to 120 nm in regionally transported air masses, which was twice that under clean conditions (Ma et al., 2017). Investigating the evolution of aerosol properties other than mass concentration during regional transport is thus useful for assessing the roles of regional and local chemistry. Such investigations are rarely conducted using the current three-dimensional chemical transport models. The current models generally account for only a part of the observed SO_4^{2-}

concentrations (Wang et al., 2014a). Heterogeneous chemistry is considered critical to improving model performance (Zheng et al., 2015; Cheng et al., 2016; Li et al., 2018). The treatment of heterogeneous chemistry is likely another source of modeling uncertainty. The heterogeneous reaction parameters are rarely related to the key parameters such as mixing state and aerosol water contents in previous studies.

From November 15 to December 15, 2016, a field campaign was carried out in Beijing within the framework of the UK-China Air Pollution & Human Health (APHH) project. Details can be seen in Shi et al. (2018). Aerosol properties such as the size distribution, number concentration, and mixing states were simultaneously measured in China. APHH-Beijing aimed to explore the sources and processes affecting urban atmospheric pollution in Beijing. In this study, we used the NAQPMS to simulate aerosol properties in the campaign period as a part of the APHH research. To improve model performance, the NAQPMS was updated by incorporating an advanced particle microphysics (APM) module that explicitly accounts for the microphysical process (Chen et al., 2014) and a new heterogeneous chemistry scheme (Li et al., 2018). The hybrid single-particle Lagrangian integrated trajectory model (HYSPLIT) was also employed to explicate the evolution of aerosol properties (e.g., mixing state, number concentration, and size distribution). Detailed analysis about the transport of precursors or secondary products, and heterogeneous reactions was mainly focused on sulfate, as recent studies indicated that sulfate is a key driver for severe haze events (Huang et al., 2014; Zheng et al., 2015). Crucially, the effects of regional transport and heterogeneous chemistry of SO_2 on aerosol properties were quantified. To our knowledge, this is the first study to distinguish the contributions of transport of SIA itself and its precursors to $PM_{2.5}$ in Beijing, and combine trajectories with microphysical properties evolution. We believe that this study is helpful to understanding the causes of haze in this megacity cluster.

2 Model description and methodology

2.1 Model description

The Nested Air Quality Prediction Model System (NAQPMS) developed by the Institute of Atmospheric Physics, Chinese Academy of Sciences (IAP/CAS) is a three-dimensional Eulerian terrain-following chemical transport model. WRFv3.6.1, driven by Final Analysis (FNL) data from the National Centers for Environmental Prediction (NCEP), provides the meteorology field for the NAQPMS. The NAQPMS includes emission, horizontal and vertical advection and diffusion, dry and wet deposition, and chemical (including gas, aqueous, and heterogeneous) reaction processes (Wang et al., 2001; Li et al., 2012; Li et al., 2018). In the model, aqueous chemistry happens only in cloud water. Heterogeneous chemistry reactions happen on aerosol aqueous layer and are related with aerosol liquid water. It also incorporates online source tagging, process analysis, an online WRF coupler, and other techniques (Wu et al., 2017; Wang et al., 2014b). The Carbon Bond Mechanism version-Z (CBMZ) is used for gas-phase chemistry mechanisms. The thermodynamic model ISORROPIAI1.7 is used to calculate the composition and phase state of an NH_4^+–SO_4^{2-}–NO_3^-–Cl^-–Na^+–H_2O inorganic aerosol system (Nenes et al., 1998). Six secondary organic aerosols (SOA) are managed using a two-product module. Further details of the NAQPMS can be found in the studies of Li et al. (2013, 2014, 2017), and numerous subsequent papers have been published describing recent updates.

To accurately describe aerosol properties (e.g., number concentration, size distribution, and mixing states), an advanced multitype, multicomponent, size-resolved microphysics (APM) module is coupled to the NAQPMS (Chen et al., 2014). APM explicitly describes microphysical aerosol processes, including nucleation, condensation, evaporation, coagulation, thermodynamic equilibrium with local humidity, hygroscopic growth, and dry and wet deposition (Yu and Luo, 2009), and it has already been applied in the global GEOS-Chem model (Ma et al., 2014). In the updated NAQPMS, 40 sectional bins covering 0.0012–12 μm were used to represent

142 secondary particle distribution (SO_4^{2-}, NO_3^-, NH_4^+, and secondary organic aerosols)
143 (Chen et al., 2014). The size distribution of BC and primary organic aerosol was
144 represented using 28 section bins. Other primary particles such as dust and sea salt were
145 represented using four bins. The coating of secondary species on primary particles (sea
146 salt, BC, OC, and dust) was explicitly simulated using a scheme that dynamically
147 calculates the aerosol aging time with an hourly resolution on the basis of aerosol
148 microphysics. Mixing state is assumed to be semi-external. Primary particles coated
149 with SIA or SOA are considered as core-shell mixing while nucleated secondary
150 particle is internally mixed (Chen et al., 2014). The mass concentrations of coating
151 species were also tracked in the model. Chen et al. (2017) employed the updated
152 NAQPMS and revealed that the daytime aging time of BC in Beijing can be less than
153 2 hours in winter. This is much less than the fixed aging time scale of 1.2 days that has
154 been stipulated in previous studies (Liu et al. 2009) but is close to observed levels (2–
155 4 hours) (Peng et al. 2016). Li et al. (2018) further developed a heterogeneous chemical
156 scheme based on mixing states to reproduce the chemical transformation of gaseous
157 precursors on aerosol surface, which largely altered the sizes and hygroscopicity of
158 particles. Heterogeneous chemistry includes oxidation of S(IV) on aqueous layer of
159 aerosols and it is parameterized according to the scheme of Li et al. (2018). Comparison
160 with long-term observations has proven that the updated NAQPMS can successfully
161 estimate aerosol mass and the number concentration, size distribution, mixing states,
162 and BC aging time in China (Li et al., 2017b, 2018; Chen et al., 2014, 2017).

163 Distinguishing the contributions of the transport of SIA itself and its precursors to
164 $PM_{2.5}$ is always difficult (Sun et al., 2014; Li et al., 2014, 2017; Ying et al., 2014). These
165 contributions have generally been named regional transport in studies; this leads to
166 ambiguity in regional transport. In this study, we divided the secondary species (e.g.,
167 SIA) in the i^{th} receptor region into four parts: 1) SIA locally produced from the i^{th} region
168 locally emitted precursors (LC); 2) SIA chemically formed in other regions from the i^{th}
169 region locally emitted precursors (LTC); 3) SIA chemically formed in the transport
170 pathway to the i^{th} receptor region from precursors emitted in the j^{th} source region (RTC);

and 4) SIA produced in the j^{th} region from precursors emitted in the j^{th} source region (RLC).

An online tracer-tagging module in the NAQPMS was used to resolve the contributions from LC, LTC, RTC, and RLC. The module is capable of tracing both the emission regions of precursors and the formation regions of secondary aerosols. First, the mass contribution from the locations in which SIA was formed, called C_2, was tagged. The mass contribution from precursors emitted in different locations, called C_1, was then tagged. More technical details can be found in the studies of Li et al. (2014) and Wu et al. (2017). The following equation can be employed to calculate the degree of chemical conversion during transport (TC):

$$\mathrm{TC} = \sum_{i=1}^{n}(C_{1i} - C_{2i} \times CC_i) \quad (1)$$

Where i means region, n is the total number of regions, and n is 10 in this study. C_{1i} refers to the absolute mass concentration transported to the receptor site, produced by precursors emitted in region i;

C_{2i} refers to the absolute mass concentration formed in region i and transported to receptor site;

CC_i refers to the local contribution ratio of precursors in region i;

$C_{2i} \times CC_i$ refers to the absolute mass transported to receptor site and generated at region *i* by chemical conversion of precursors released at region *i*. When $i = 1$, it refers to LC; when $i \neq 1$, $\sum_{i=2}^{n} C_{2i} \times CC_i$ refers to RLC;

$C_{1i} - C_{2i} \times CC_i$ is the mass concentration generated in all regions except *i* by chemical conversion of the precursors released at region *i* and finally transported to the receptor site. When $i = 1$, it refers to LTC; when $i \neq 1$, $\sum_{i=2}^{n}(C_{1i} - C_{2i} \times CC_i)$ refers to RTC.

In this study, 10 regions according to administrative division are selected for source tagging (Fig. 1c), six of which—Chengde, Zhangjiakou, and Qinhuangdao (NHB); Beijing (BJ); Tianjin (LT); Hengshui, Xingtai, and Handan (SHB); Baoding and Shijiazhuang (WHB); and Tangshan, Langfang, and Cangzhou (EHB)—are parts of the Beijing–Tianjin–Hebei (BTH) area. Henan (HN), Shandong (SD), Shanxi (SX), and other regions (OT) are regions outside the BTH area.

2.2 Model configuration

Simulation was conducted from November 10 to December 15, 2016, and the first 5 days were set aside as a spin-up period. The three nested model domains were shown in Fig. 1a. The horizontal resolutions were 27, 9, and 3 km from the coarsest to innermost domain. The first level of the NAQPMS was approximately 20 m in height, and there were approximately 17 layers under 2 km.

To quantitatively assess the contribution of primary emissions, traditional chemistry reactions (gas-phase and aqueous chemistry reactions), and heterogeneous chemistry to sulfate, three sensitivity simulations were conducted. The baseline scenario (Base) involving all heterogeneous reactions considered primary sulfate emissions and its results were used for model verification and source apportionment analysis. Control 1 (C1) involved all heterogeneous reactions but did not consider primary sulfate emissions. Compared with Base, Control 2 (C2) excluded the heterogeneous reactions of SO_2. Base–C2 represents the effect of heterogeneous reactions on sulfate. Base–C1 represents contribution of primary sulfate emissions.

The HYSPLIT model was used to analyze the trajectories of air masses (Draxler and Hess, 1998). The calculated trajectories are helpful to resolving the evolution of aerosol properties in the transport pathway by extracting the simulated results by the NAQPMS along trajectories. In this study, the same meteorology data (obtained hourly data of the third domain) used in the NAQPMS were employed to perform trajectory analysis; this avoided the errors caused by inconsistency between the two models (the NAQPMS and HYSPLIT).

2.3 Emission inventory

The anthropogenic emissions were obtained from the 0.25° × 0.25° Multi–resolution Emission Inventory for China (MEIC), and the base year was 2016 for BTH (http://www.meicmodel.org/publications.html). In addition, observation data collected at sites within BTH were used to update the MEIC on the basis of their latitude and

longitude information. Biomass burning emissions were taken from the Fire Inventory from NCAR (National Center for Atmospheric Research) (Wiedinmyer et al., 2011). Primary sulfate was assumed to constitute 5% of SO_2 emissions in the original MEIC inventory. Cao et al. (2014), Wang et al. (2009), Zheng et al. (2013), and Ma et al. (2015) discovered that primary sulfate comprised large amounts of primary $PM_{2.5}$ from industrial, power, and residential emissions in the main form of $(NH4)_2SO_4$ through in situ measurement of source profiles. Thus, we took 40%, 6% and 15% of primary $PM_{2.5}$ from industrial, power and residential emissions, respectively, as primary sulfate emissions in the inventory. Figure 1b displays the hourly primary $PM_{2.5}$ emission rate.

2.4 Observations

The surface meteorological parameters were obtained from the China Meteorological Administration, whereas the vertical profiles of meteorological parameters were obtained from the University of Wyoming (http://weather.uwyo.edu/upperair/sounding.html). Observations of $PM_{2.5}$, SO_2, NO_2, and O_3 concentrations were obtained from the China National Environmental Monitoring Center (http://www.cnemc.cn/). Aerosol components (including organic matters [OM], sulfate, nitrate, and ammonium) were measured in situ at Beijing using an Aerodyne high-resolution time-of-flight aerosol mass spectrometer. Details of the instruments can be found in the study by Sun et al. (2015). A seven-wavelength Aethalometer (AE33, Magee Scientific Corp.) was used to measure BC at Beijing (Xie et al., 2018). The OC/EC in aerosol was measured by a field semi-online OC/EC analyzer from Sunset Laboratory Inc. (USA) with a $PM_{2.5}$ cyclone inlet at Tianjin and Lang Fang (Gao et al., 2016). Two same ambient ion monitors (AIM; Model URG 9000D, URG Corporation) were used to measure hourly concentrations of water-soluble ions in $PM_{2.5}$, including NH_4^+, Na^+, K^+, Ca^{2+}, Mg^{2+}, SO_4^{2-}, NO_3^- and Cl^- at TJ and LF (Gao et al., 2016). The particle number size distributions at ground level were obtained using a scanning mobility particle sizer (SMPS) with a time resolution of 5 min. Details of the instruments can be found in the study by Du et al. (2017). All data

in this study are presented in Beijing local time (UTC + 8 h).

3 Model validation

3.1 $PM_{2.5}$ mass and number concentrations and aging degrees

The time series of simulated and observed $PM_{2.5}$ in different cities of BTH from November 15 to December 15, 2016, are illustrated in Fig. 2. During the study period, six regional haze episodes were identified, namely, November 15–20 (Ep1), November 23–26 (Ep2), November 28–30 (Ep3), December 2–4 (Ep4), December 6–8 (Ep5), December 10–12 (Ep6). The $PM_{2.5}$ mass concentration frequently exceeded 200 μg m^{-3} and the average concentration reached 120 μg m^{-3} during episodes. Haze usually formed in several hours; for example, the increasing rate of $PM_{2.5}$ reached 200 μg m^{-3} h^{-1} and lasted approximately 12 hours in Tangshan. These observed haze patterns were generally reproduced by the NAQPMS. The correlation coefficient (R) between the observation and simulation in most cities was 0.6–0.8, and 60%–80% of simulation results were within a factor of 2 of the observation. The mean fractional bias (MFB) and mean fractional error (MFE) ranged from −0.07 to 0.7, meeting the criteria of MFB $\leq$ 0.6 and MFE $\leq$ 0.75 (Boylan et al., 2006). The simulation did however underestimate $PM_{2.5}$ in Beijing and Baoding for Ep2. This was caused by the failure of the mineral aerosol transport simulation. Compared with other cities in the cluster, Beijing and Baoding are closer to the Gobi Desert, a major dust source in East Asia, and they are thus more easily affected by dust storm transport. Pan et al. (2018) found a pronounced peak in the size distribution at 4–5 μm for Ep2 in Beijing. The concentrations of Ca^{2+} was 7 times the campaign averages (Fig. S1).

The aerosol components in Beijing, Langfang, and Baoding are compared in Fig. 3. In general, the simulation largely reproduced the variation in primary and secondary aerosols. In particular, the rapid increase in SIA during Ep1, Ep2, and Ep4 was captured by the simulation. Interestingly, the NAQPMS underestimated the sulfate concentration in Beijing during Ep2 and Ep4, but the nitrate and ammoniate concentrations during

these two episodes were successfully reproduced. This was related to the transport of mineral dust (Ep2) and local emissions (Ep4). As discussed in the last paragraph, Beijing had high mineral loadings for Ep2, which provided a favorable medium for chemical transformation of anthropogenic SO_2 into sulfate in the form of $CaSO_4$ or $MgSO_4$ (Wang et al., 2018b;Wang et al., 2017c). Underestimation of the sulfate concentration for Ep4 may have been caused by local emissions in Beijing. As illustrated in Fig. 3, the simulation failed to reproduce the sharp increase in both sulfate and BC in Beijing during this episode. This is different from the case of Ep2, in which sulfate was underestimated but BC was favorably reproduced. Wang et al. (2009) and Ma et al. (2015) found that sulfate accounted for 40% and 6.6% of primary $PM_{2.5}$ emissions from industry and power plants, which also emit a large amount of BC. This sharp increase in BC was a local-scale episode. In Langfang, a site 50–60 km from Beijing, both the observed and simulated BC concentration increased slowly to 20 μg m^{-3}, which is much less than that in Beijing (45 μg m^{-3}). The monthly emissions employed in this study made it difficult to capture these short-term local-scale emission changes. The simulated SO_2 concentrations are compared with the observations in Fig. S2, and the normalized mean bias (NMBs) were less than 40%.

The number size distribution is critical to examining aerosol evolution during haze episodes (Ma et al., 2017). In this study, both the simulation and observation revealed a rapid increase in the GMD from 50 to approximately 120 nm during the initial stages of episodes in Beijing (Fig. 4). The observed mean number concentration of aerosols (dN/dlogDp) showed a unimodal distribution and was mainly concentrated in the Aitken mode (25–100 nm) and accumulation mode (100–1,000 nm). The highest concentration was approximately 1.8×10^4 cm^{-3} at a 100-nm diameter. These patterns were favorably reproduced by the simulation. The simulated number concentrations were underestimated in 10–60 nm by 20%–30% and overestimated in 80–150 nm by 20%. This indicated that the model needs to be improved regarding its treatment of new particle formation and the volatility of primary organic aerosols.

Herein, the aging degree of BC is represented by the mass ratio of coating to BC

311 (R_{BC}), which has been widely used in previous studies (Oshima et al., 2009; Collier et
312 al., 2018). Figure 11 shows that the mean simulated R_{BC} in Beijing was 4.5 and 5.0 in
313 the entire study period and during pollution episodes, respectively, which are extremely
314 close to the observations (~5.0 and 5.1) (Wang et al., 2018a). The high performance of
315 the model in terms of mass and number concentrations, compositions, and the aging
316 degree of aerosols gives us confidence for analyzing aerosol evolution during transport
317 in the megacity cluster centered on Beijing.

318 **3.2 Meteorology**

319 The simulated wind direction and speed coincided with the observations for the
320 haze episodes. In particular, the model captured low wind speeds, and the moments
321 when the wind shifted direction were well reproduced (Fig. S3). Regarding relative
322 humidity and temperature, WRF performed high values of R (0.68–0.93) and low
323 NMBs (−0.51 to 0.44) (Table S1). In particular, the high relative humidity during Ep1
324 was well reproduced. Inversion layers were present during the initial stage of haze
325 formation (Fig. S4). The height of the inversion layers varied among episodes. During
326 Ep1 and Ep6, strongly elevated inversion layers were present between 1 and 2 km,
327 whereas the inversion layers were close to the surface during other episodes.
328 Temperature inversion is favorable for pollution accumulation, and the model
329 reproduced this feature favorably. In sum, the high performance of the meteorological
330 simulation gave us confidence for $PM_{2.5}$ simulation.

331 # 4 Results and discussion

332 **4.1 Source apportionment of surface $PM_{2.5}$**

333 The simulated spatial distribution of average surface $PM_{2.5}$ levels and the wind
334 vector during the six haze episodes are shown in Fig. 5. In general, two types of patterns
335 were observed. The first pattern corresponded to Ep1, Ep4, and Ep6 and reflected that
336 a highly polluted belt with $PM_{2.5}$ over 200 μg m^{-3} extended from the southwest to the

northeast along the Taihang mountain range. In the second pattern (Ep2, Ep3, and Ep5), the $PM_{2.5}$ level of 150–200 μg m^{-3} was concentrated in three northern cities (Beijing, Tianjin, and Tangshan). In the other cities, the $PM_{2.5}$ mass concentrations ranged from 75 μg m^{-3} to 115 μg m^{-3}, indicating a light pollution level according to the Technical Regulation on Ambient Air Quality Index (on trial).

Figure 6 shows the contributions of regional transport and local emissions to average $PM_{2.5}$, primary aerosol (PA, BC and non-organic primary $PM_{2.5}$), and SIA levels in different cities during the study period. The contribution of local emissions was more than that of regional transport to the $PM_{2.5}$ mass concentration in all cities, except Heng Shui, Cangzhou, Langfang, and Qinhuangdao; the magnitude of local emission contributions was 49%–80%. The principle reason for this was the accumulation of local PA emissions. In most cities, 64%–93% of PA originated from local emissions (Fig. 6c). In contrast to PA, the SIA contribution was dominated by regional transport of emissions in other cities (50%–87%). Even the emissions of cities outside the city cluster (e.g., Henan, Shanxi and Shandong) were transported to the megacity cluster, travelling 500–1,000 km. In Beijing, the local contribution to total $PM_{2.5}$ and PA was 74% and 94%, respectively, whereas regional transport from other cities was the major source of SIA, contributing 51%. The difference in source apportionment between PA and SIA was related to the mechanisms of PA and SIA formation. Regarding PA, the inversion layer and weak winds during stable weather conditions prevented PA transport and resulted in local-scale accumulation of PA emissions. The regional transport provided sufficient time (1–3 days) and aerosol surface for chemical transformation of precursors to SIA (Li et al., 2015; Li et al., 2017b). This also indicates that regional controls on precursors would be the most efficient way to decreasing the SIA concentration in this megacity cluster. Our results agree favorably with the observed impact of regional emission controls in Asia-Pacific Economic Cooperation China 2014. During this gathering, the SIA concentration in Beijing decreased to a greater degree than the PA concentration because of regional controls (Sun et al., 2016).

The source apportionment in haze episodes in Beijing is illustrated in Fig. 7. Regional transport contributed 14%–31% to the surface $PM_{2.5}$ mass concentration during the six episodes. The highest contribution of regional transport occurred in Ep1 and Ep5 (29% and 31% of the total $PM_{2.5}$, respectively). In Ep1 and Ep5, the contribution of the SIA originating from regional transport reached 53% and 63%, respectively. Interestingly, the regionally transported SIA had different source regions in Ep1 and Ep5. In Ep5, SX, WHB, and NHB were the dominant source regions, whereas the source regions for Ep1 were more diverse. This indicates the complexity of regional transport in this megacity cluster. Compared with the episodes in November 2015, the effects of regional transport of $PM_{2.5}$ and SIA mass concentrations were weaker in this study, which may be related to the weather system and emission controls in 2016 (Li et al., 2017b). Therefore, more studies on regional transport should be conducted to further understand regional haze formation mechanisms. In other episodes (Ep2, Ep3, Ep4, and Ep6), regional transport of surface $PM_{2.5}$, PA, OM (organic matters, sum of primary organic aerosols [POA] and secondary organic aerosols [SOA]), and SIA mass concentrations were in the range 14%–23%, 3%–12%, 3%–14%, and 30%–51%, respectively. Back trajectories and emissions source regions can be connected (Fig. S5). Taking Ep6 for example, airmass mainly came from Shandong, through SHB, WHB and finally arrived at Beijing. What's more, the height of trajectory within WHB is low, so contribution of WHB should be big, which agreed with results of Figure 7b, and source apportionment results showed that WHB contributed 24% to SIA at Beijing during Ep6.

Figure 8 presents the relative contribution of regionally transported SIA and variation of wind direction under different pollution levels in Beijing. The source regions varied considerably under different pollution levels. When Beijing is controlled by strong northerly wind, NHB and SX are the main source regions, contributing up to 30% and 19%, resulting in clean conditions (SIA < 50 μg m^{-3}). When Beijing is mainly affected by southerly wind (southeast, south and southwest), WHB, EHB and SD become the main source regions, contributing 27%, 13% and 15%, respectively. Strong

emissions of source regions lead to heavier pollution level in Beijing. When Beijing is dominated by weak southeast wind, contribution from far regions like HN and SD increases. Continuous transport and accumulation lead to severe pollution (SIA > 150 μg m^{-3}). This indicates that wider regional emission control is necessary to reduce severe pollution.

4.2 Impact of regional transport of sulfate and its precursors on Beijing

Quantifying the impact of regional transport of sulfate and its precursors is a crucial task. Sun et al. (2014) considered sulfate formed outside Beijing as regionally transported sulfate, and they estimated that its contribution reached 75% during winter haze episodes. By tagging emissions regions of precursors in models and ignoring where secondary aerosols were formed, Li et al. (2017) and Timmermans et al. (2017) estimated the contribution of transport to be 40%–50%. These estimated contributions of regional transport are different in physical meaning, which may confuse policymakers. In this study, we divided the sulfate mass concentration in Beijing into four parts, LC, LTC, RLC, and RTC as described in Sect. 2.1. The regional transport defined by Sun et al. (2014) was LTC + RLC + RTC, whereas in the studies by Li et al. (2017) and Timmermans et al. (2017), it was RLC + RTC. In this study, we employed RLC + RTC as representing regional transport.

Figure 9a shows the contributions of LC, LTC, RLC, and RTC to the daily average sulfate concentration in Beijing during the study period. RTC and LC were the dominant sources of sulfate, contributing 71%–89% in total. The contributions of RTC ranged from 29% in Ep6 to 59% in Ep2, and contributions of LC were 30%–42%. RTC dominated the regional transport over the whole period, which indicates that chemical conversions in the transport pathway of SO_2 were critical to haze formation. Notably, the LTC contribution was comparable with that of LC in Ep3, Ep4, and Ep6. This suggests that the SO_2 emitted in Beijing was blown away and formed sulfate outside Beijing. And recirculation of air masses can be convinced by HYSPLIT trajectories

(Fig. S6). Take trajectories at 23:00 on December 12 [LST] for example, air masses were blown away Beijing by southwesterly, through Chengde, Tianjin and Langfang, and finally tarvelled back to Beijing. These formed sulfates may have been blown back to Beijing under certain weather conditions and were previously considered regional transport. The contribution of LTC also largely explains the difference in estimated regional transport contributions between Sun et al. (2014) and Li et al. (2017). In the present study, LTC + RLC + RTC accounted for 58%–70% of the sulfate concentration in the six episodes, which is relatively similar to the estimation (75%) of Sun et al. (2014), which was based on the observed hourly increase rate of local sulfate concentration.

In the initial and subsequent pollution stages, LC, LTC, and RTC showed different patterns in Beijing. In Ep1, local contributions dominated before the sulfate concentration increased rapidly (November 15 and 16). In particular, sulfate blown back to Beijing from its local emissions (LTC) made a larger contribution (35%) than RTC (25%). In the rapid rising phase of sulfate (November 17 and 18), contribution of RTC increased from 25% to 47%. LC was also significant and contribution increased considerably from 37% to 41%. These two parts (LC and RTC) explained the rapid formation of sulfate in Beijing. This suggests that the joint control of local and regional SO_2 emissions is essential for preventing the rapid formation of haze in this region, which is receiving considerable attention and eliciting widespread interest among the researchers and policymakers (Sun et al., 2014; Ma et al., 2017; Li et al., 2017b). This feature is also reflected in Fig. 9b. Under clear conditions (sulfate < 20 μg m^{-3}), the local contributions (LC and LTC) were positively correlated with the sulfate mass concentration. In total, they contributed 40%–60% of the sulfate mass concentration. The ratio of LC to LTC was approximately 2:1. Under moderate sulfate levels (20 μg m^{-3} < sulfate < 35 μg m^{-3}), the local contribution was lower—particularly the LTC—leading to a ratio of LC to LTC of approximately 8. Contribution of sulfate formed in the regional transport pathway (RTC) significantly increased from 40% to 65%. Under heavy pollution levels (> 35 μg m^{-3}), the LC contributed up to 50% due to extremely

stable boundary layers. Our results are consistent with those of Ma et al. (2017), in which regional transport and local heterogeneous chemistry were qualitatively discovered to make high contributions to initial and subsequent pollution stages.

4.3 Evolution of aerosol properties in Beijing during haze episodes

Aerosol properties such as the particle size and aging degree can change dramatically on haze days because of fresh emissions, subsequent chemical conversions, and regional transport, which strongly affect regional radiation and climate (Cappa et al., 2012). As illustrated in Fig. 4b, the GMD of aerosols in Beijing increased remarkably to approximately 120 nm during the six haze episodes, compared with 50 nm under clean conditions. Two stages were identified: an initial rising stage and a sustained increase stage. In the initial stage, the GMD of aerosols increased by 50–60 nm within several hours, and the GMD then remained at 100–120 nm for several days in the subsequent elevated pollution stage. This GMD increase during the initial stage was mainly caused by the increase of accumulation-mode particles with diameters of 100–1,000 nm and Aitken-mode particles (Fig. 10). Under clean conditions (SIA < 50 μg m^{-3}), the average contributions of the three modes (nucleation, Aitken, and accumulation modes) to the number concentration were comparable, although the number of nucleation-mode particles decreased with SIA concentration. Under light-moderate pollution conditions (50 < SIA < 150 μg m^{-3}), the proportion of accumulation-mode particles significantly increased from 35% to 60%, whereas the proportion of Aitken-mode particles slowly decreased. As discussed in previous sections, regional transport played a dominant role during the initial stage. This indicates that condensation, coagulation, and chemical transformation in the transport pathway increased the number of particles with a diameter range of 100–1,000 nm. Finally, the contributions of Aitken-mode and accumulation-mode particles remained stable under the heavy-pollution conditions (SIA >150 μg m^{-3}).

Aging processes play a critical role in the growth of particles during haze episodes. According to observations, a significant coating of secondary components on BC was found in the study period (Wang et al., 2018a). Figure 11 presents a time series of the simulated R_{BC}, which is a favorable indicator of the aging degree (Oshima et al., 2009; Collier et al., 2018). Higher R_{BC} indicates that BC had undergone a greater degree of aging. In this study, the simulated R_{BC} was 2–10, with an average value of 4.5. Under pollution conditions, R_{BC} was higher than that under clean conditions, with an average value of 5.0. R_{BC} in Beijing even exceeded 10.0 in some extremely severe pollution events, which is close to observations of remote sites (Wang et al., 2017a; Massoli et al., 2015) and aged particles (Cappa et al., 2012). Urban aerosols usually have a lower R_{BC} because of fresh emissions and high R_{BC} in this study indicates that Beijing aerosol particles were more aged during the haze episodes. On clean days, R_{BC} ranged from 2 to 5, with an average of 2.8. This is similar to the R_{BC} of vehicle emissions (<3) (Liu et al, 2017), indicating that Beijing is affected by local emission. Vehicle emissions contributed 70% of BC in downtown Beijing in 2016 after strict controls on coal burning had been implemented (Kebin He, personal communication).

Figure 12 shows the evolution of R_{BC}, GMD , and region source of BC along the transport pathway from the source region to Beijing during the six haze episodes. Aerosol properties including number concentration along transport per six hours are shown in Table S2. The transport pathway was calculated using the HYSPLIT model. The figure clearly shows that the aerosol properties changed considerably along the transport pathway. In Ep1, the GMD of aerosols was only 97 nm at the initial site of the 24 h back trajectories (T_{-24}). At a larger transport distance, the diameters of aerosol particles were markedly increased to 128 nm in the middle (T_{-12}) and 134 nm at the final site (T_0) of the back trajectory. R_{BC} increased from 3.6 at T_{-24} to 8.7 at Beijing (T_0) because of BC being coated during the transport. This indicates that BC underwent considerable aging and increased in size while moving along the transport pathway. Similar characteristics were discovered for Ep3–6. In Ep3, Ep4, Ep5, and Ep6, the GMD in Beijing (T_0) was 126, 117, 124, and 116 nm, respectively, compared with 96,

95, 99, and 111 nm in the middle point of transport (T_{-12}). R_{BC} also increased to 4.6–7.6. An exception was Ep2, in which the GMD (106 nm) and R_{BC} (3.8) at the final ending site (Beijing, T_0) were lower than those 6 h previously (T_{-6}). Regional transport contributed 95% of BC at T_{-6}, whereas local emissions accounted for 87% of BC at T_0. The number concentration was smaller at T_{-6} than that at T_0. Therefore, we conclude that regional transport of aged aerosols led to a high GMD at T_{-6}, and that the addition of locally emitted fresh air caused a high number concentration but low GMD at T_0. In clean areas, such as at T_{-24} in Ep5, R_{BC} was higher than 10 and the GMD was considerably smaller.

4.4 Impact of heterogeneous chemistry on sulfate mass concentration

Current models generally account for a part of the observed SO_4^{2-} concentrations in China (Wang et al., 2014a). Heterogeneous chemistry on aerosol surfaces under high relative humidity has been considered a potential missing source of sulfate formation (Cheng et al., 2016; Zheng et al., 2015; Li et al., 2017a; Tang et al., 2016b). Li et al. (2018) developed a simple parameterization of heterogeneous chemistry and discovered that SO_2 uptake on aerosols partly closed the gap between simulation and observation. In their study, uptake coefficients were dependent on the aerosol core and shell species, shell thickness, and amount of aerosol liquid water. Zheng et al. (2013) and Yang et al. (2014) measured local source profiles, and they reported that primary sulfate from industry and power plants accounted for a large fraction of PA. Researchers also found that household coal burning can emit certain amounts of sulfate (Zhang et al., 2018).

In this study, we examined the contributions of gas (SO_2 + OH) and aqueous chemistry, heterogeneous chemistry, and primary sulfate emissions to the sulfate mass concentration in Beijing (Fig. 13). In Ep1, under high relative humidity, the contribution of heterogeneous chemistry was 33%. Primary emissions exerted an effect mostly under

light to moderate pollution levels (sulfate < 20 μg m^{-3}), whereas heterogeneous chemistry played a crucial role under high pollution levels (sulfate > 30 μg m^{-3}). The contributions of gas and aqueous chemistry were largely consistent under all pollution conditions (~30%). This indicates that high relative humidity and aerosol loading accelerated the SO_2 chemical transformation. Interestingly, the contribution of heterogeneous chemistry was markedly higher when the sulfate mass concentration exceeded the threshold of 20 μg m^{-3}. Under high relative humidity and mass concentration conditions, a higher aerosol surface area resulting from hygroscopic growth and haze particles under high RH (60–80%) with aqueous shell due to phase transition provided a favorable media for heterogeneous reactions (Tie et al., 2017; Sun et al., 2018). The aforementioned threshold is relatively similar to that during the haze episodes in the winter of 2013 (Li et al, 2018). For policymakers, implementing measures to prevent the sulfate concentration from exceeding this threshold is essential. Such measures would be effective for avoiding extremely high sulfate levels. In other episodes, heterogeneous chemistry was depressed because of the low relative humidity (< 70%). Gas and aqueous chemistry and primary emissions contributed 35%–40% and 58%–61%, respectively. It should be noted that failure of the model to simulate mineral dust led to underestimation of the sulfate level in Ep2. The interaction between SO_2 and alkaline dust can contribute considerably to the sulfate concentration.

5 Conclusions

The contributions of regional transport to haze episodes over a megacity cluster centered on Beijing have been under debate in recent decades. Investigating the evolution of aerosol properties along the transport pathway may provide more information on how researchers can improve the accuracy of regional transport and chemistry impact assessments. To address one of the aims of the APHH 2016 winter campaign, we employed a Eulerian chemical transport model (NAQPMS) and a Lagrangian trajectory model (HYSPLIT) to assess the evolution of aerosols—in terms of the number concentration, size distribution, and aging degree—in Beijing during six

haze episodes between November 15 and December 15, 2016. The transport of sulfate and its precursors was also quantitatively investigated.

The results demonstrated that regional transport contributed 14%–31% to the surface $PM_{2.5}$ mass concentration in Beijing during the six episodes, with a monthly average contribution of 26%. Regarding aerosol components, 30%–62% of the SIA in Beijing were regionally transported, whereas few PAs (< 10%) were contributed from emissions in other regions. Source regions differed between episodes. During high-pollution periods, WHB, SD, and EHB were the main source regions of SIA regionally transported to Beijing, whereas NHB and SX made greater contributions under clean and light pollution conditions. This indicates the complexity of regional transport in this megacity cluster.

The chemical transformation of SO_2 along the transport pathway from source regions except Beijing to Beijing (RTC) was the major source of SO_4^{2-} regional transport and was more critical than the transport of sulfate formed in source regions except Beijing (RLC). Compared with sulfate that was chemically transformed from Beijing-emitted SO_2 and then blown back to Beijing (LTC), contribution of sulfate produced in Beijing from Beijing-emitted SO_2 (LC) was generally greater. However, RTC markedly increased in some episodes, and it explained the rapid formation of sulfate in Beijing. This suggests that the joint control of local and regional SO_2 emissions is essential for reducing the rapid formation of haze in this region.

Aerosols became considerably aged during transport in haze episodes, which altered R_{BC} and the size distribution of number concentrations. During haze episodes, the GMD increased from less than 100 nm at the initial site to approximately 120 nm at the final site (Beijing), and R_{BC} increased from 2–4 to 4–8. The number of accumulation-mode particles with a diameter range of 100–1,000 nm increased considerably more than the number of particles of different modes. R_{BC} in Beijing during the episodes was higher than that of urban regions (Collier et al., 2018) and R_{BC} under pollution levels was close to that in remote regions (Wang et al., 2017a), which

indicates that BC in Beijing under pollution conditions was more aged and thus more likely to affect radiation and circulation.

Contributions from different pathways to sulfate in Beijing were also examined. In episodes with high humidity (Ep1), the average contributions of gas and aqueous chemistry, heterogeneous chemistry, and primary sulfate were comparable. Primary emissions mostly had an effect under light to moderate pollution levels, whereas heterogeneous chemistry played a relatively crucial role under high pollution levels during Ep1. In other episodes (Ep2, Ep3, Ep4, Ep5, and Ep6), gas and aqueous chemistry and primary emissions contributed 35%–40% and 58%–61%, respectively.

Author contributions.

HD and JL designed the idea and experiments. HD performed all the model runs, did the analysis and wrote the paper. JL prepared the emissions data and contribued to the paper writing. ZW and XC contributed to the model development; YS, PF, JJL and JG provided observation data. YW contributed to data processing. All authors discussed the paper.

Acknowledgements:

This work was supported by the Natural Science Foundation of China (41571130034; 91544227; 91744203; 41225019; 41705108) and the Chinese Ministry of Science and Technology (2018YFC0213205 and 2017YFC0212402).

References

Anderson, H. R., Atkinson, R., Balbus, J., Brauer, M., Chapman, R., Chowdhury, Z.: Outdoor Air Pollution and Health in the Developing Countries of Asia: A Comprehensive Review, Special Report 18, Health Effects Institute, Boston, Massachusetts, 2010.

Boylan, J. W., & Russell, A. G.: PM and light extinction model performance metrics, goals, and criteria for three-dimensional air quality models, Atmospheric Environment, 40(26), 4946-4959, https://doi.org/10.1016/j.atmosenv.2005.09.087, 2006.

Cao J.: $PM_{2.5}$ and environment. Science Press, 2014.

Cappa, C. D., Onasch, T. B., Massoli, P., Worsnop, D. R., Bates, T. S., Cross, E. S., … Zaveri, R.

A.: Radiative Absorption Enhancements Due to the Mixing State of Atmospheric Black Carbon, Science, 337(6098), 1078–1081, https://doi.org/10.1126/science.1223447, 2012.

Chen, X., Li, X., Yuan, X., Zeng, G., Liang, J., Li, X., . . . Chen, G.: Effects of human activities and climate change on the reduction of visibility in Beijing over the past 36years, Environ Int, 116, 92-100, https://doi.org/10.1016/j.envint.2018.04.009, 2018.

Chen, X., Wang, Z., Li, J., & Yu, F.: Development of a regional chemical transport model with size-resolved aerosol microphysics and its application on aerosol number concentration simulation over china, Scientific Online Letters on the Atmosphere Sola, 10, 83-87, https://doi.org/10.2151/sola.2014-017, 2014.

Chen, X., Wang, Z., Yu, F., Pan, X., Li, J., & Ge, B., et al.: Estimation of atmospheric aging time of black carbon particles in the polluted atmosphere over central-eastern china using microphysical process analysis in regional chemical transport model. Atmospheric Environment, 163, 44-56, https://doi.org/10.1016/j.atmosenv.2017.05.016, 2017.

Cheng, Y., Zheng, G., Wei, C., Mu, Q., Zheng, B., & Wang, Z., et al: Reactive nitrogen chemistry in aerosol water as a source of sulfate during haze events in china, Science Advances, 2(12), https://doi.org/10.1126/sciadv.1601530, 2016.

Collier, S., Williams, L. R., Onasch, T. B., Cappa, C. D., Zhang, X., & Russell, L. M., et al: Influence of emissions and aqueous processing on particles containing black carbon in a polluted urban environment: insights from a soot particle-aerosol mass spectrometer, Journal of Geophysical Research Atmospheres, 123(12), 6648-6666, https://doi.org/10.1002/2017jd027851, 2018.

Draxler, R. R., & Hess, G. D: An overview of the HYSPLIT 4 modeling system for trajectories, dispersion, and deposition, Australian Meteorological Magazine, 47(4), 295-308, 1998.

Du, W., Zhao, J., Wang, Y., Zhang, Y., Wang, Q., & Xu, W., et al: Simultaneous measurements of particle number size distributions at ground level and 260 m on a meteorological tower in urban Beijing, china, Atmospheric Chemistry & Physics, 17(11), 6797-6811, https://doi.org/10.5194/acp-17-6797-2017, 2017.

Gao, J., Peng, X., Chen, G., Xu, J., Shi, G. L., Zhang, Y. C., and Feng, Y. C.: Insights into the chemical characterization and sources of $PM_{2.5}$ in Beijing at a 1-h time resolution, The Science of the total environment, 542, 162-171, 10.1016/j.scitotenv.2015.10.082, 2016.

Han, B., Zhang, R., Yang, W., Bai, Z., Ma, Z., & Zhang, W: Heavy haze episodes in Beijing during January 2013: inorganic ion chemistry and source analysis using highly time-resolved measurements from an urban site, Science of the Total Environment, 544, 319-329, https://doi.org/10.1016/j.scitotenv.2015.10.053, 2016.

Huang, R. J., Zhang, Y., Bozzetti, C., Ho, K. F., Cao, J. J., Han, Y., . . . Prevot, A. S: High secondary aerosol contribution to particulate pollution during haze events in China, Nature, 514(7521), 218-222, https://doi.org/10.1038/nature13774, 2014.

Hyslop, N. P.: Impaired visibility: the air pollution people see, Atmospheric Environment, 43(1), 182-195, https://doi.org/10.1016/j.atmosenv.2008.09.067, 2009.

Lee, A. K. Y., Chen, C. L., Liu, J., Price, D. J., Betha, R., Russell, L. M., Zhang, X., and Cappa, C. D.: Formation of secondary organic aerosol coating on black carbon particles near vehicular emissions, Atmos. Chem. Phys., 17(24), 15055-15067, https://doi.org/10.5194/acp-17-15055-2017, 2017.

Li, G., Bei, N., Cao, J., Huang, R., Wu, J., & Feng, T., et al.: A possible pathway for rapid growth of sulfate during haze days in china, Atmospheric Chemistry & Physics, 17(5), 3301-3316, https://doi.org/10.5194/acp-17-3301-2017, 2017a.

Li, J., Chen, X., Wang, Z., Du, H., Yang, W., & Sun, Y., et al.: Radiative and heterogeneous chemical effects of aerosols on ozone and inorganic aerosols over east Asia, Science of the Total Environment, 622-623, 1327, https://doi.org/10.1016/j.scitotenv.2017.12.041, 2018.

Li, J., Du, H., Wang, Z., Sun, Y., Yang, W., & Li, J., et al.: Rapid formation of a severe regional winter haze episode over a mega-city cluster on the North China Plain, Environmental Pollution, 223, 605-615, https://doi.org/10.1016/j.envpol.2017.01.063, 2017b.

Li, J., Han, Z.: A modeling study of severe winter haze events in Beijing and its neighboring regions, Atmospheric Research, 170, 87-97, https://doi.org/10.1016/j.atmosres.2015.11.009, 2016.

Li, J., Wang, Z., Huang, H., Min, H. U., Meng, F., & Sun, Y., et al.: Assessing the effects of trans-boundary aerosol transport between various city clusters on regional haze episodes in spring over east china, Tellus, 65(1), 60-73, https://doi.org/10.3402/tellusb.v65i0.20052, 2013.

Li, J., Yang, W., Wang, Z., Chen, H., Hu, B., & Li, J., et al.: A modeling study of source–receptor relationships in atmospheric particulate matter over northeast Asia. Atmospheric Environment, 91(7), 40-51, https://doi.org/10.1016/j.atmosenv.2014.03.027, 2014.

Li, J., Wang, Z.F., Zhuang, G., Luo, G., Sun, Y., Wang, Q.: Mixing of Asian mineral dust with anthropogenic pollutants over East Asia: a model cast study of a super-dust storm in March 2010. Atmos. Chem. Phys. 12 (16), 7591-7607. https://dx.doi.org/10.5194/acp-12-7591-2012, 2012.

Li, P., Yan, R., Yu, S., Wang, S., Liu, W., & Bao, H.: Reinstate regional transport of $PM_{2.5}$ as a major cause of severe haze in Beijing, Proc Natl Acad Sci U S A, 112(21), E2739-2740, https://doi.org/10.1073/pnas.1502596112, 2015.

Liu, D., Whitehead, J., Alfarra, M. R., Reyes-villegas, E., Spracklen, D. V., & Reddington, C. L., et al.: Black-carbon absorption enhancement in the atmosphere determined by particle mixing state, Nature Geoscience, 10(3), 184-188, https://doi.org/10.1038/ngeo2901, 2017.

Liu, X., Zhang, Y., Jung, J., Gu, J., Li, Y., & Guo, S., et al.: Research on the hygroscopic properties of aerosols by measurement and modeling during CAREBeijing-2006, Journal of Geophysical Research Atmospheres, 114(16), 4723-4734, https://doi.org/10.1029/2008jd010805,2009.

Ma, Q., Wu, Y., Zhang, D., Wang, X., Xia, Y., Liu, X., . . . Zhang, R.: Roles of regional transport and heterogeneous reactions in the $PM_{2.5}$ increase during winter haze episodes in Beijing, Sci Total Environ, 599-600, 246-253, https://doi.org/10.1016/j.scitotenv.2017.04.193, 2017.

Ma, X., & Yu, F.: Seasonal variability of aerosol vertical profiles over east us and west Europe:

GEOS-Chem/APM simulation and comparison with CALIPSO observations, Atmospheric Research, 140-141(31), 28-37, https://doi.org/10.1016/j.atmosres.2014.01.001, 2014.

Ma, Z., Liang YP, Zhang J.: $PM_{2.5}$ profiles of typical sources in Beijing, Acta Science Circumstantiae, 35(12), 4043-4052, https://doi.org/10.13671/j.hjkxxb.2015.0584, 2015.

Massoli, P., Onasch, T. B., Cappa, C. D., Nuamaan, I., Hakala, J., & Hayden, K., et al.: Characterization of black carbon containing particles from soot particle aerosol mass spectrometer measurements on the R/V Atlantis during CalNex 2010, Journal of Geophysical Research Atmospheres, 120(6), 2575-2593, https://doi.org/10.1002/2014jd022834, 2015.

Nenes, A., Pandis, S.N., Pilinis, C.: ISORROPIA: A new thermodynamic equilibrium model for multiphase multicomponent inorganic aerosols, Aquat. Geochem. 4(1), 123-152. https://dx.doi.org/10.1023/A:1009604003981, 1998.

Oshima, N., Koike, M., Zhang, Y., Kondo, Y., Moteki, N., & Takegawa, N., et al.: Aging of black carbon in outflow from anthropogenic sources using a mixing state resolved model: model development and evaluation, Journal of Geophysical Research Atmospheres, 114(D6), https://doi.org/10.1029/2008jd010680, 2009.

Pan, X., Ge, B., Wang Z., Tian, Y., et al.: Synergistic effect of water-soluble species and relative humidity on morphological changes of aerosol particles in Beijing mega-city during severe pollution episodes, Atmos. Chem. Phys. Discuss, 1-24, https://doi.org/10.5194/acp-2018-623, 2018.

Peng J, Hu M, Guo S, et al.: Markedly enhanced absorption and direct radiative forcing of black carbon under polluted urban environments, Proc Natl Acad Sci USA, 113(16), 4266-4271, https://doi.org/10.1073/pnas.1602310113, 2016.

Shi, Z., Vu, T., and Kotthaus, S.: Introduction to Special Issue-In-depth study of air pollution sources and processes within Beijing and its surrounding region(APHH-Beijing), Atmos. Chem. Phys. Discuss, 1-62, https://doi.org/10.5194/acp-2018-922, 2018.

Sun, Y., Chen, C., Zhang, Y., Xu, W., Zhou, L., Cheng, X., . . . Wang, Z.: Rapid formation and evolution of an extreme haze episode in Northern China during winter 2015, Sci Rep, 6(1), 27151. https://doi.org/10.1038/srep27151, 2016.

Sun, Y., Du, W., Wang, Q., Zhang, Q., Chen, C., & Chen, Y., et al. Real-time characterization of aerosol particle composition above the urban canopy in Beijing: insights into the interactions between the atmospheric boundary layer and aerosol chemistry, Environmental Science & Technology, 49(19), 11340-11347, https://doi.org/10.1021/acs.est.5b02373, 2015.

Sun, Y., Jiang, Q., Wang, Z., Fu, P., Li, J., Yang, T., & Yin, Y.: Investigation of the sources and evolution processes of severe haze pollution in Beijing in January 2013, Journal of Geophysical Research: Atmospheres, 119(7), 4380-4398, https://doi.org/10.1002/2014jd021641, 2014.

Tang, G., Zhang, J., Zhu, X., Song, T., Münkel, C., Hu, B., et al.: Mixing layer height and its implications for air pollution over Beijing, China, Atmos. Chem. Phys., 16(4), 2459-2475, https://doi.org/10.5194/acp-16-2459-2016, 2016a.

733 Tang, M. J., Larish, W. A., Fang, Y., Gankanda, A., and Grassian, V. H.: Heterogeneous Reactions
734 of Acetic Acid with Oxide Minerals: Effects of Mineralogy and Relative Humidity, J. Phys.
735 Chem. A, 120(28), 5609-5616, https://doi.org/10.1021/acs.jpca.6b05395, 2016b.

736 Tie, X., Huang, R. J., Cao, J., Zhang, Q., Cheng, Y., Su, H., . . . O'Dowd, C. D.: Severe Pollution in
737 China Amplified by Atmospheric Moisture, Sci Rep, 7(1), https://doi.org/10.1038/s41598-017-
738 15909-1, 2017.

739 Timmermans, R., Kranenburg, R., Manders, A., Hendriks, C., Segers, A., & Dammers, E., et al.:
740 Source apportionment of $PM_{2.5}$ across china using LOTOS-EUROS, Atmospheric
741 Environment, 164, 370-386, https://doi.org/10.1016/j.atmosenv.2017.06.003, 2017.

742 Wang, J., Liu, D., Ge, X., Wu, Y., Shen, F., Chen, M., . . . Sun, Y.: Characterization of black carbon-
743 containing fine particles in Beijing during wintertime, Atmospheric Chemistry and Physics
744 Discussions, 1-25, https://doi.org/10.5194/acp-2018-800, 2018a.

745 Wang, J., Zhang, Q., Chen, M. D., Collier, S., Zhou, S., & Ge, X., et al.: First chemical
746 characterization of refractory black carbon aerosols and associated coatings over the Tibetan
747 plateau (4730 m a.s.l), Environmental Science & Technology, 51(24), 14072-14082,
748 https://doi.org/10.1021/acs.est.7b03973, 2017a.

749 Wang, S., Zhao, X., Li, X., Wei, W., Hao, J.: Study on fine particle emission characteristics of
750 industrial coal-fired chain furnace. Environmental Science (Chines), 30 (4), 963-968,
751 https://doi.org/10.3321/j.issn:0250-3301.2009.04.004, 2009.

752 Wang, Y. Y., Liu, F. S., He, C. L., Bi, L., Cheng, T. H., Wang, Z. L., Zhang, H., Zhang, X. Y., Shi,
753 Z. B., and Li, W. J.: Fractal Dimensions and Mixing Structures of Soot Particles during
754 Atmospheric Processing, Environ Sci Tech Let, 4, 487-493, 10.1021/acs.estlett.7b00418,
755 2017b.

756 Wang, Y., Zhang, Q., Jiang, J., Zhou, W., Wang, B. Y., He, K. B., . . . Xie, Y. Y.: Enhanced sulfate
757 formation during china's severe winter haze episode in January 2013 missing from current
758 models, Journal of Geophysical Research Atmospheres, 119(17), 10425-10440,
759 https://doi.org/doi: 10.1002/2013jd021426, 2014a.

760 Wang, Z., Maeda, T., Hayashi, M., Hsiao, L.F., Liu, K.Y.: A nested air quality prediction modeling
761 system for urban and regional scales, application for high-ozone episode in Taiwan, Water, Air,
762 Soil Pollut, 130, 391-396, https://dx.doi.org/10.1023/A:1013833217916. 2001.

763 Wang, Z., Jie, L., Wang, Z., Yang, W. Y., Tang, X., & Ge, B. Z., et al.: Modeling study of regional
764 severe hazes over mid-eastern China in January 2013 and its implications on pollution
765 prevention and control, Science China Earth Sciences, 57(1), 3-13,
766 https://dx.doi.org/10.1007/s11430-013-4793-0, 2014b.

767 Wang, Z., Pan, X., Uno, I., Li, J., Wang, Z., Chen, X., Fu, P., Yang, T., Kobayashi, H., Shimizu, A.,
768 Sugimoto, N., and Yamamoto, S.: Significant impacts of heterogeneous reactions on the
769 chemical composition and mixing state of dust particles: A case study during dust events over
770 northern China, Atmospheric Environment, 159, 83-91, 10.1016/j.atmosenv.2017.03.044,
771 2017c.

772 Wang, Z., Pan, X., Uno, I., Chen, X., Yamamoto, S., Zheng, H., Li, J., and Wang, Z.: Importance of
773 mineral dust and anthropogenic pollutants mixing during a long-lasting high PM event over
774 East Asia, Environmental pollution, 234, 368-378, 10.1016/j.envpol.2017.11.068, 2018b.

775 Wiedinmyer, C., Akagi, S. K., Yokelson, R. J., & Emmons, L. K.: The fire inventory from NCAR
776 (FINN) – a high resolution global model to estimate the emissions from open burning,
777 Geoscientific Model Development, 4(3), 625-641, https://doi.org/10.5194/gmd-4-625-2011,
778 2011.

779 Wu, J. B., Wang, Z., Wang, Q., Li, J., Xu, J., & Chen, H., et al.: Development of an on-line source-
780 tagged model for sulfate, nitrate and ammonium: A modeling study for highly polluted periods
781 in Shanghai, China. Environmental Pollution, 221, 168-179,
782 https://doi.org/10.1016/j.envpol.2016.11.061, 2017.

783 Xie, C., Xu, W., Wang, J., Wang, Q., Liu, D., Tang, G., Chen, P., Du, W., Zhao, J., Zhang, Y., Zhou,
784 W., Han, T., Bian, Q., Li, J., Fu, P., Wang, Z., Ge, X., Allan, J., Coe, H., and Sun, Y.: Vertical
785 characterization of aerosol optical properties and brown carbon in winter in urban Beijing,
786 China, Atmospheric Chemistry and Physics Discussions, 1-28, 10.5194/acp-2018-788, 2018

787 Yang, H. H.: Filterable and condensable fine particulate emissions from stationary sources, Aerosol
788 & Air Quality Research, 14(7), 2010-2016, https://doi.org/10.4209/aaqr.2014.08.0078, 2014.

789 Yang, Y., Liu, X., Qu, Y., Wang, J., An, J., & Zhang, Y., et al.: Formation mechanism of continuous
790 extreme haze episodes in the megacity Beijing, China, in January 2013. Atmospheric Research,
791 155, 192-203, https://doi.org/10.1016/j.atmosres.2014.11.023, 2015.

792 Yang, Y., Wang, H., Smith, S. J., Easter, R., Ma, P. L., Qian, Y., . . . Rasch, P. J.: Global source
793 attribution of sulfate concentration and direct and indirect radiative forcing, Atmospheric
794 Chemistry and Physics, 17(14), 8903-8922, https://doi.org/10.5194/acp-17-8903-2017, 2017a.

795 Yang, Y., Wang, H., Smith, S. J., Ma, P.-L., & Rasch, P. J.: Source attribution of black carbon and
796 its direct radiative forcing in China, Atmospheric Chemistry and Physics, 17(6), 4319-4336,
797 https://doi.org/10.5194/acp-17-4319-2017, 2017b.

798 Ying, Q. Wu, L. Zhang, H.: Local and inter-regional contributions to $PM_{2.5}$ nitrate and sulfate in
799 China, Atmos. Environ., 94, 582-592, https://doi.org/10.1016/j.atmosenv.2014.05.078, 2014.

800 Yu, F., & Luo, G.: Simulation of particle size distribution with a global aerosol model: contribution
801 of nucleation to aerosol and CCN number concentrations, Atmospheric Chemistry & Physics,
802 9(20), 7691-7710, https://doi.org/10.5194/acp-9-7691-2009, 2009.

803 Zhang, Y., Yuan, Q., Huang, D., and Kong, S.: Direct Observations of Fine Primary Particles From
804 Residential Coal Burning: Insights Into Their Morphology, Composition, and Hygroscopicity,
805 Journal of Geophysical Research, 123, 12964–12979, 2018.

806 Zhao, X. J., Zhao, P. S., Xu, J., Meng, W., Pu, W. W., Dong, F., . . . Shi, Q. F.: Analysis of a winter
807 regional haze event and its formation mechanism in the North China Plain, Atmospheric
808 Chemistry and Physics, 13(11), 5685-5696, https://doi.org/10.5194/acp-13-5685-2013, 2013.

809 Zheng, B., Zhang, Q., Zhang, Y., He, K. B., Wang, K., Zheng, G. J., & Kimoto, T.: Heterogeneous

chemistry: a mechanism missing in current models to explain secondary inorganic aerosol formation during the January 2013 haze episode in North China, Atmospheric Chemistry and Physics, 15(4), 2031-2049, https://doi.org/10.5194/acp-15-2031-2015, 2015.

Zheng M., Zhang Y., Yan C., et al.: Establishment of $PM_{2.5}$ industrial source profile in Shanghai, China Environmental Science, 33(8), 1354-1359, https://doi.org/10.3969/j.issn.1000-6923.2013.08.002, 2013.

Zhu, X., Tang, G., Hu, B., Wang, L., Xin, J., & Zhang, J., et al.: Regional pollution and its formation mechanism over north China plain: a case study with ceilometer observations and model simulations, Journal of Geophysical Research Atmospheres, 121(24), 14574-14588, https://doi.org/10.1002/2016jd025730, 2016.

842 **Figures**

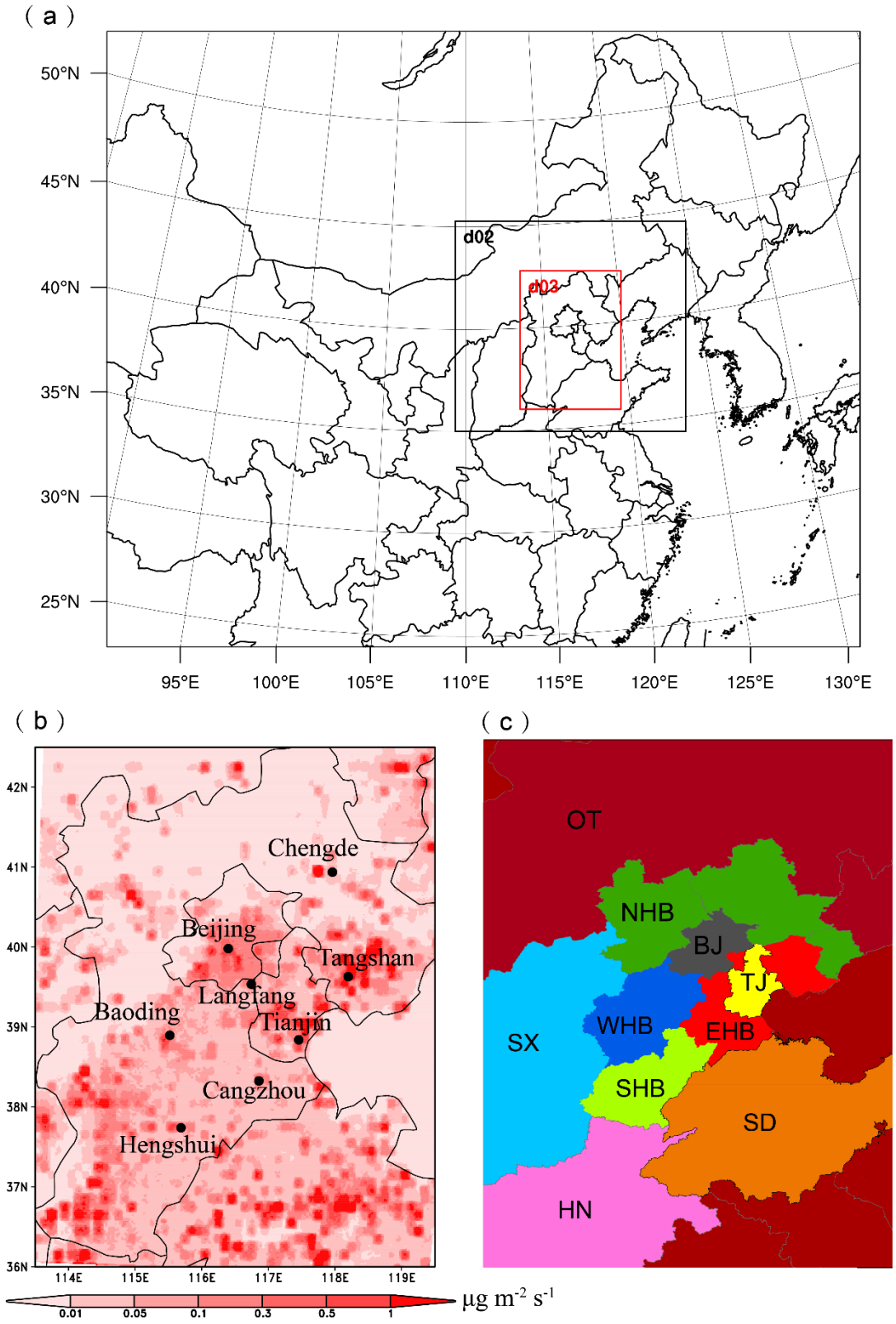

843

844 **Figure 1.** (a) Simulation domains. (b) Primary $PM_{2.5}$ emission rates of the innermost

845 domain and locations of observation sites (black dots). (c) tracer tagging regions which

are described in Table 1.

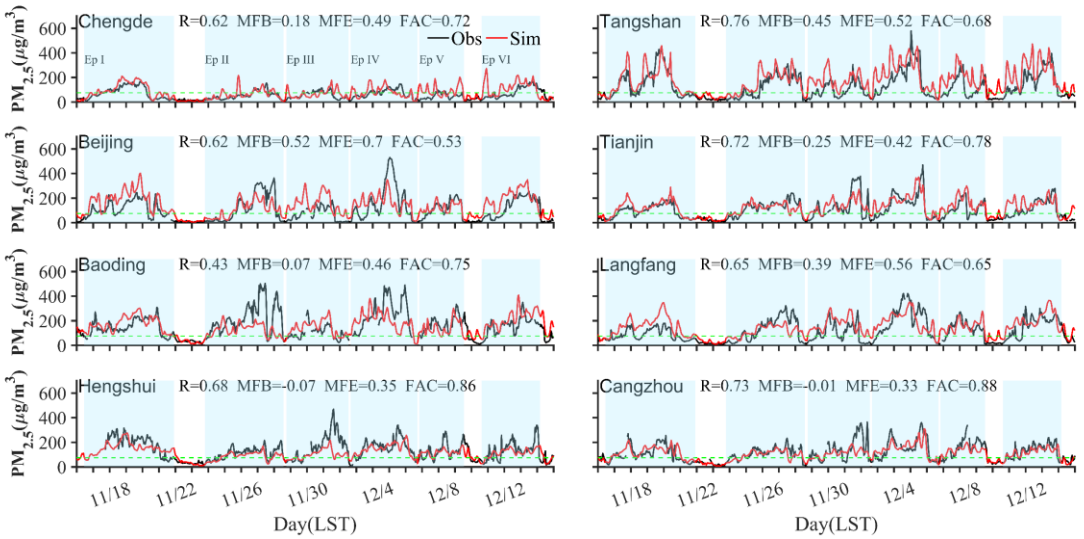

Figure 2. Comparison between the simulated and observed hourly concentrations of $PM_{2.5}$ for different sites. Black lines refer to observation and the red lines are simulation results; light blue shadows are six episodes identified; green lines mean 75 μg m^{-3}, as a criterion judging whether pollution or not.

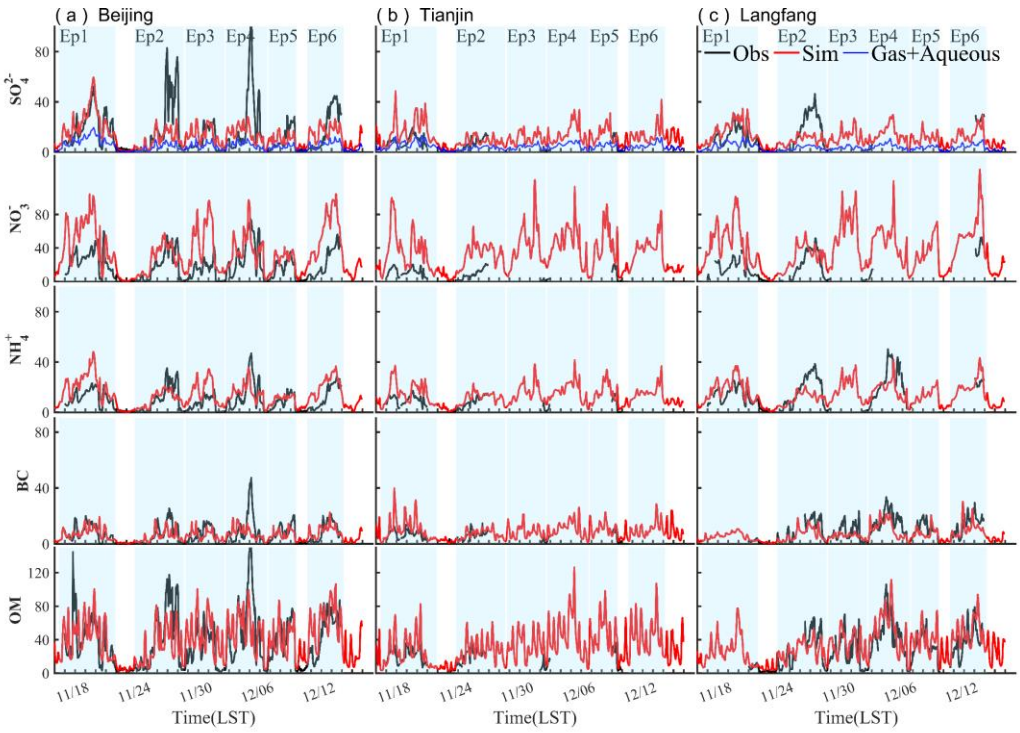

Figure 3. Comparison between the simulated (red) and observed (solid black) hourly components including sulfate, nitrate, ammonia, black carbon and organic aerosols at (a) Beijing, (b) Tianjin and (c) Langfang. Blue lines refer to sulfate produced by gas

and aqueous chemistry reactions.

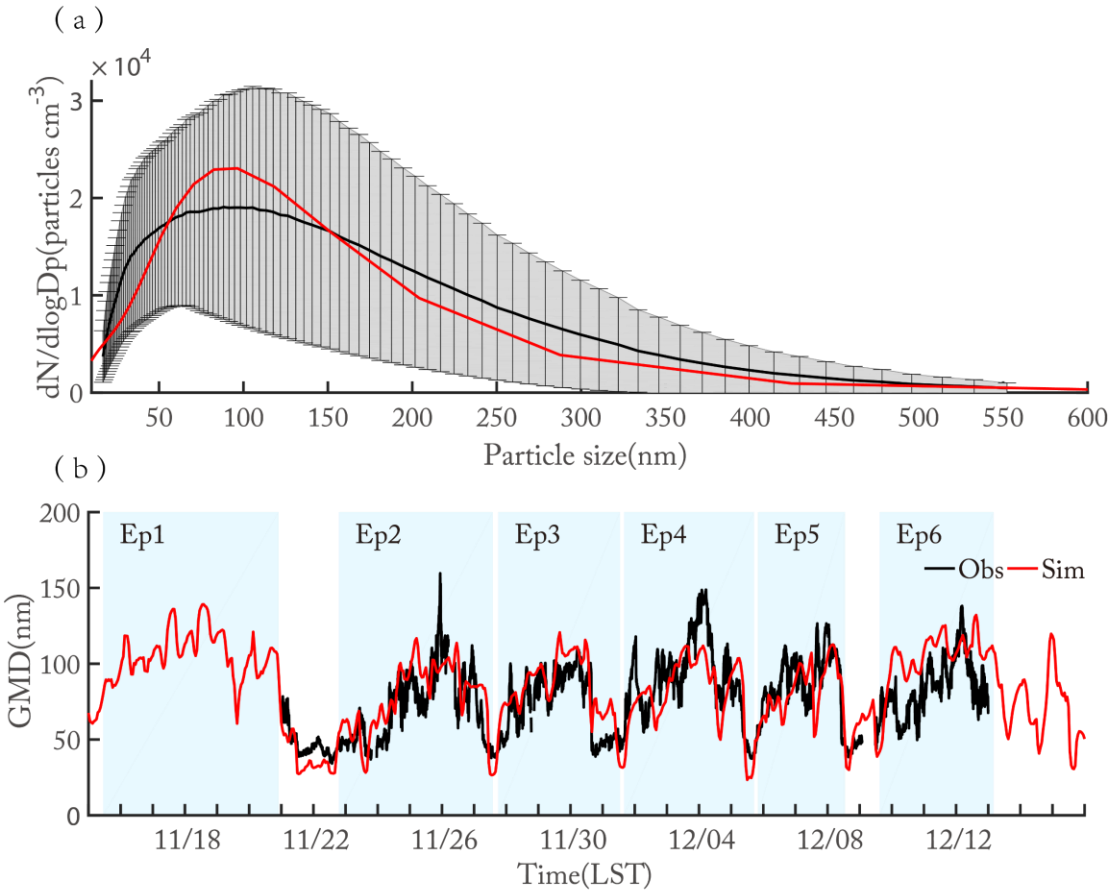

Figure 4. (a) Particle size distribution in Beijing at ground level. (b) Comparison of geometric mean diameter (GMD) for particles during range of 16–600nm between observation and simulation in Beijing. Black solid line and red solid line represent observation and simulation respectively.

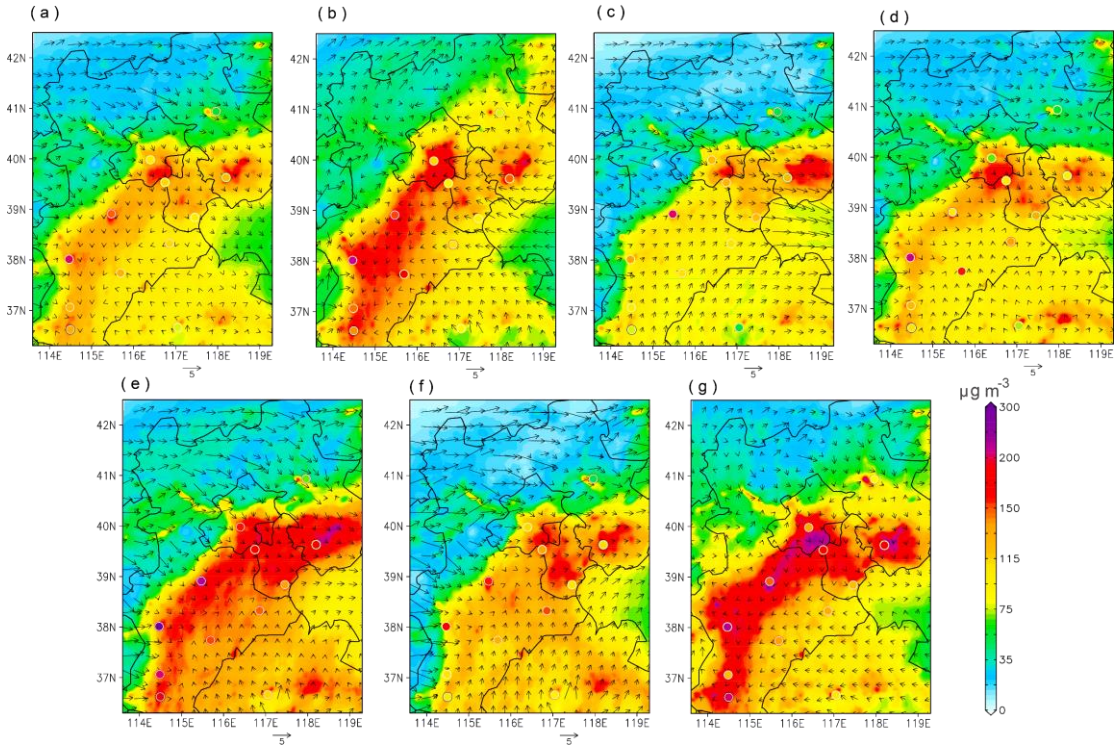

Figure 5. Spatial distribution of simulated average surface $PM_{2.5}$ (μg m^{-3}) and wind (m s^{-1}) over BTH area. (a) average of the whole study period, (b)–(g) episode average of episode1–6 identified before. Solid circles represent observations with the same color bar with simulations.

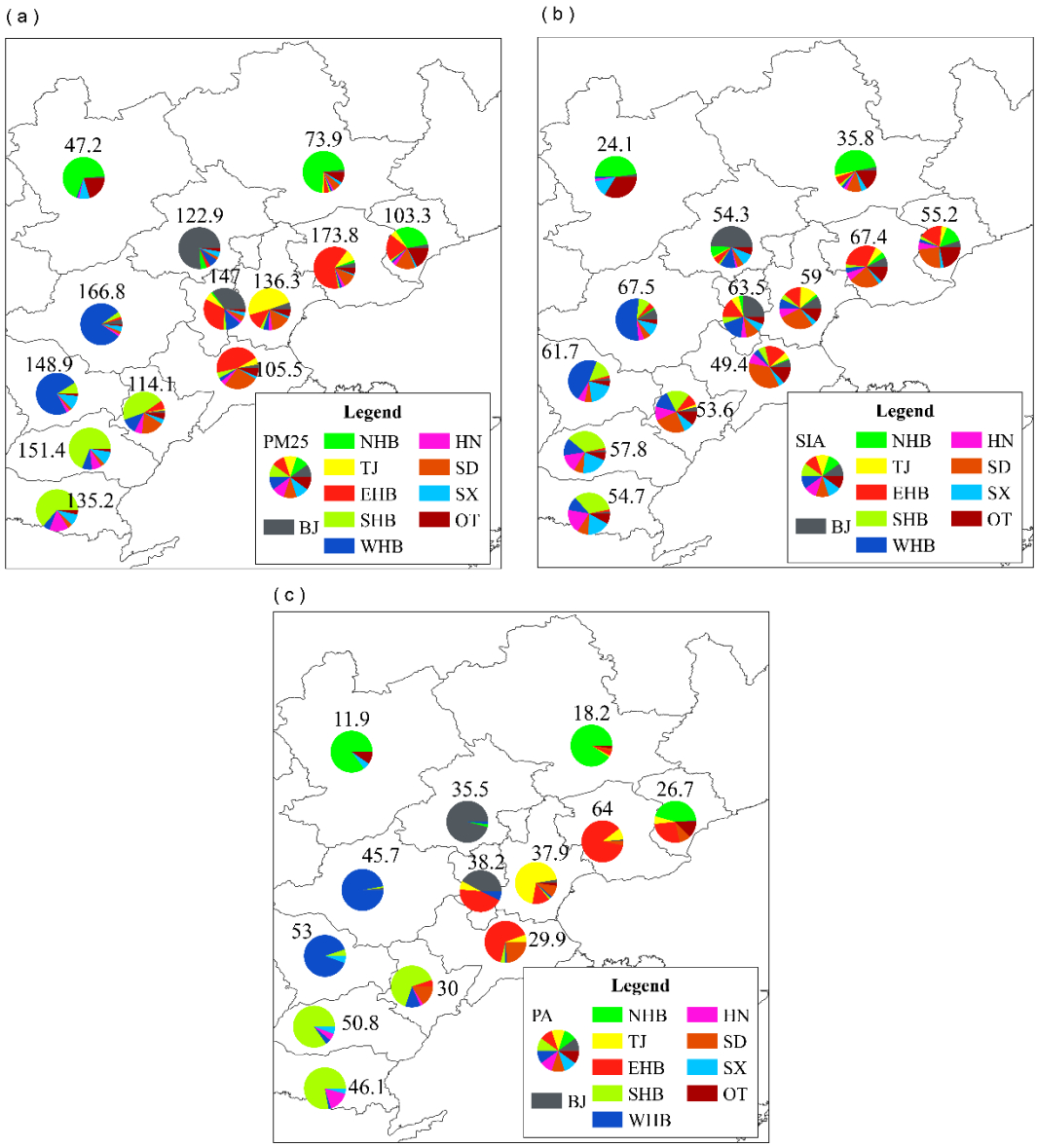

867

868 **Figure 6.** The contribution of regional transport and local emissions to the average (a)
869 total $PM_{2.5}$, (b) secondary inorganic aerosols (SIA), (c) primary aerosols (PA, BC and
870 primary $PM_{2.5}$) over BTH area. The numbers above the pie represent average
871 concentrations ($\mu g\ m^{-3}$) of certain species in certain cities.

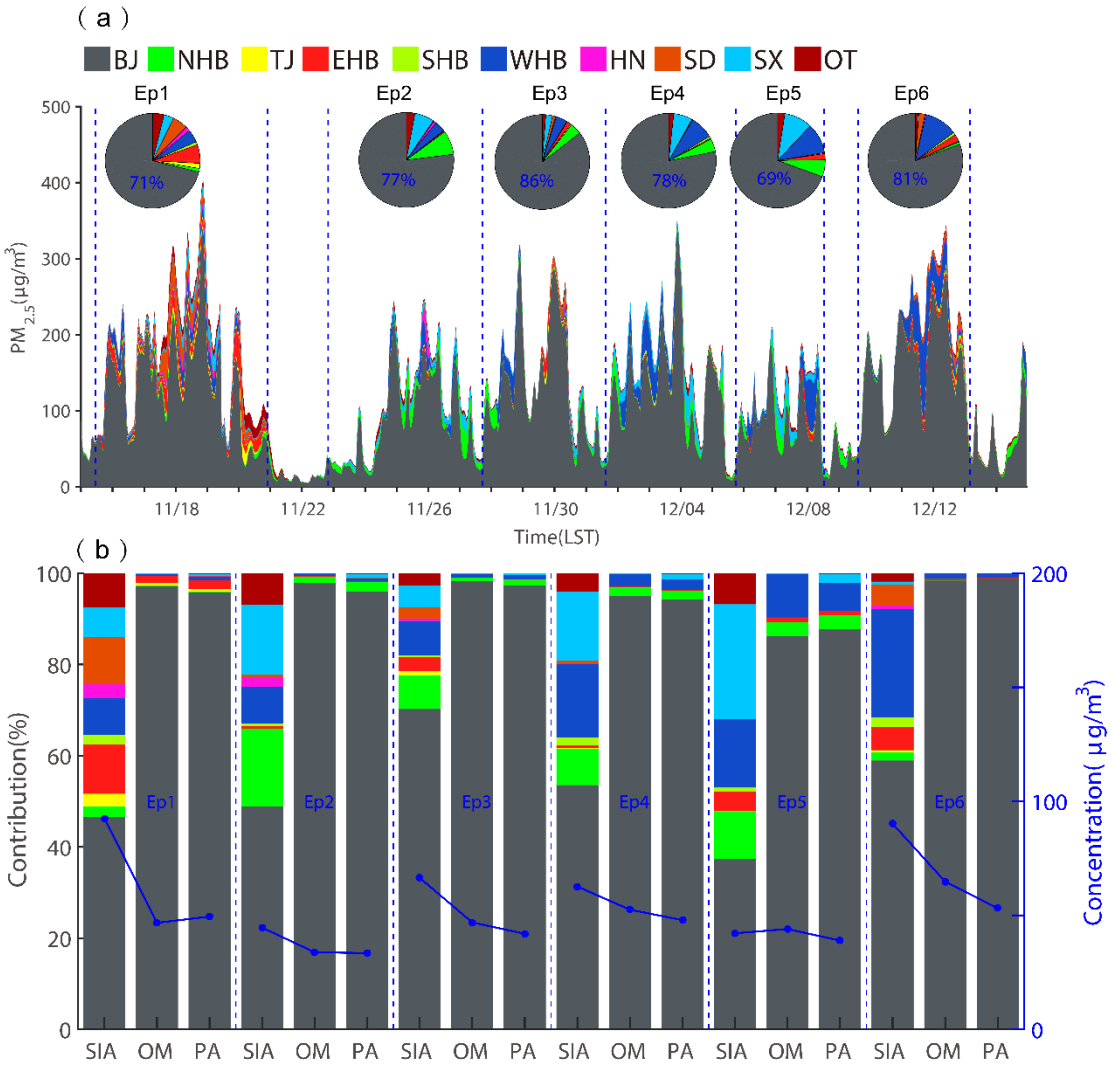

Figure 7. (a) Source contribution of $PM_{2.5}$ in Beijing and pies represent average status of each episode; (b) Relative contribution of different regions to SIA, OM and PA in Beijing at the surface layer during each episode (shaded). Concentrations are also shown (blue line).

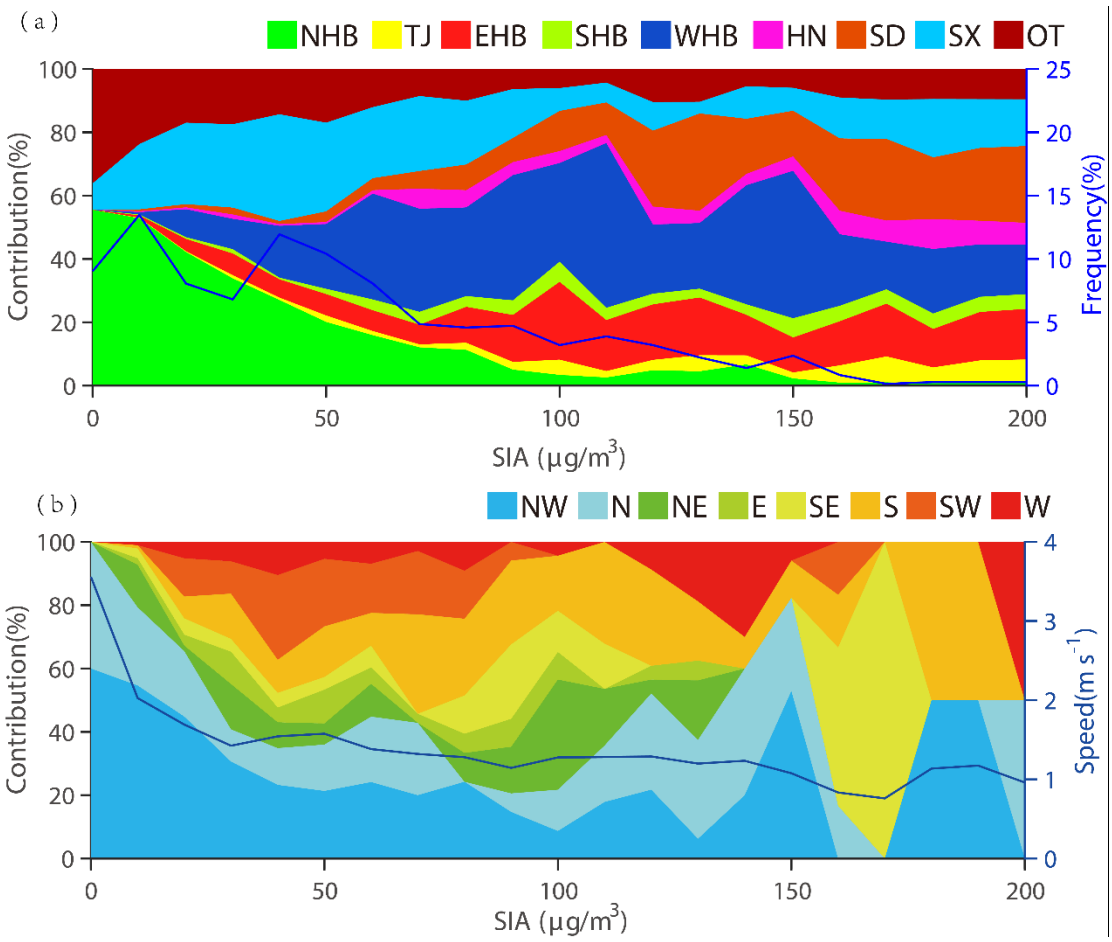

877

878 **Figure 8.** (a) Relative contribution of regionally transported SIA under different
879 pollution levels in Beijing during the whole study period; (b)Variation of wind
880 directions under different pollution levels in Beijing during the whole study period.

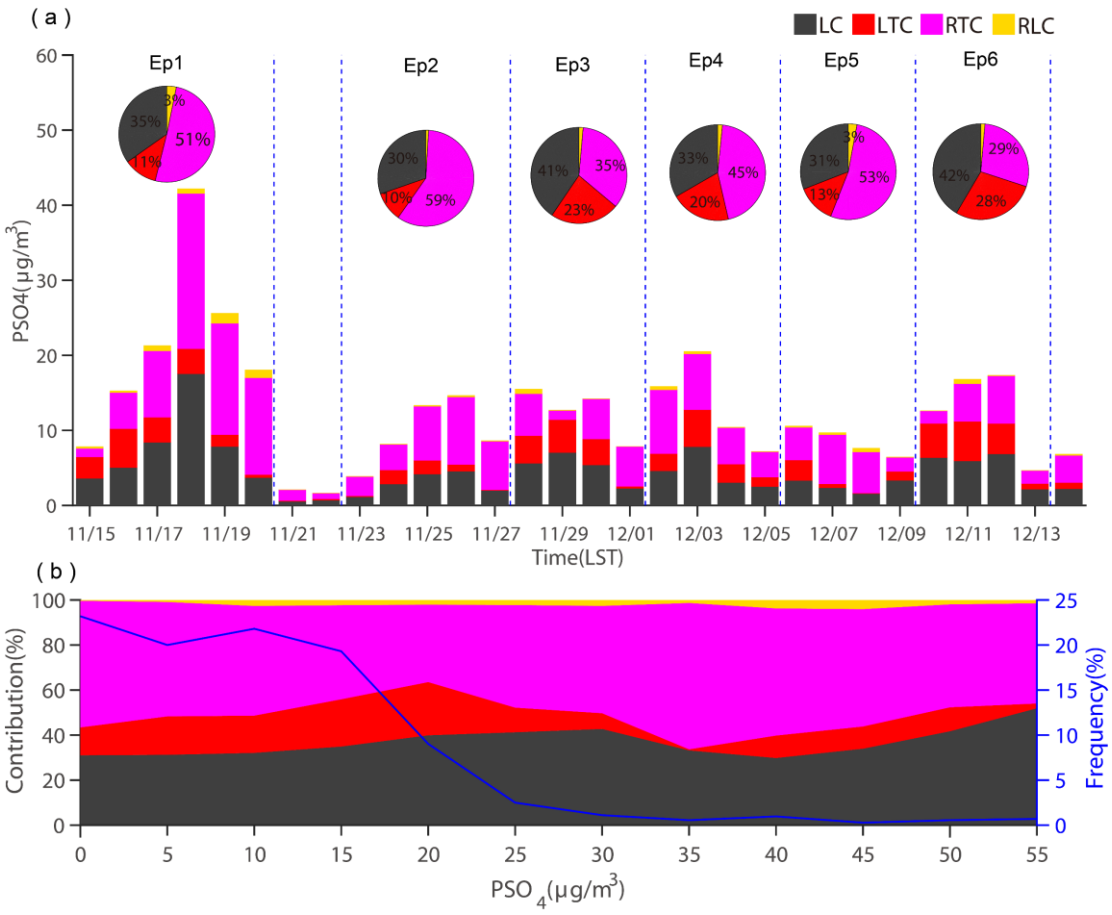

Figure 9. (a) Sources of secondary sulfate in Beijing. (b) Variation of secondary sulfate sources with surface sulfate concentration in Beijing for the whole study period. LC means sulfate locally produced from Beijing emitted SO_2; LTC refers to sulfate chemically formed in regions except Beijing from the Beijing emitted SO_2; RTC is sulfate chemically formed in the transport pathway to Beijing from SO_2 emitted in source regions except Beijing; RLC is sulfate produced in regions except Beijing from locally emitted SO_2 and transported to Beijing.

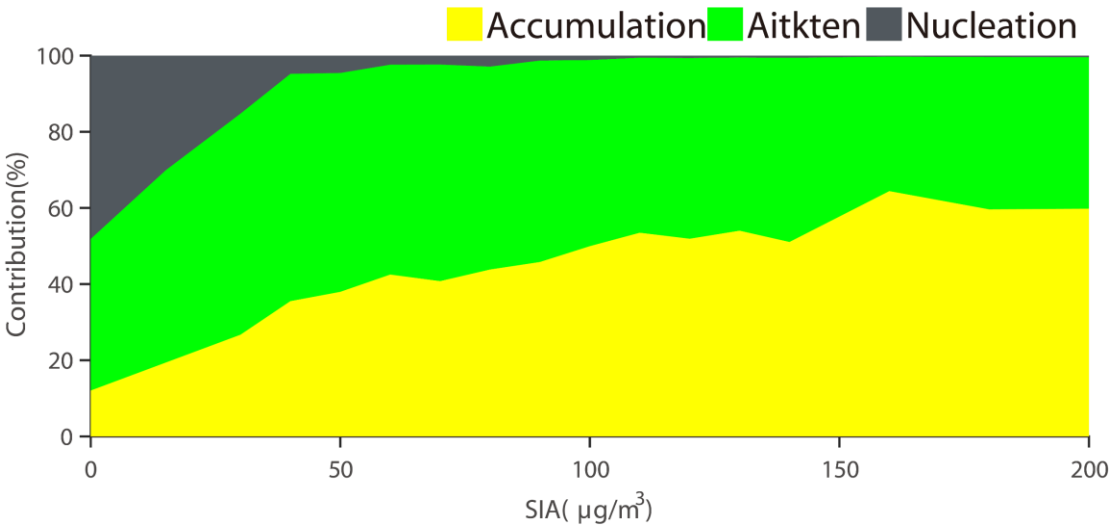

Figure 10. Variation of number concentration fraction of particles with SIA in Beijing during whole study period.

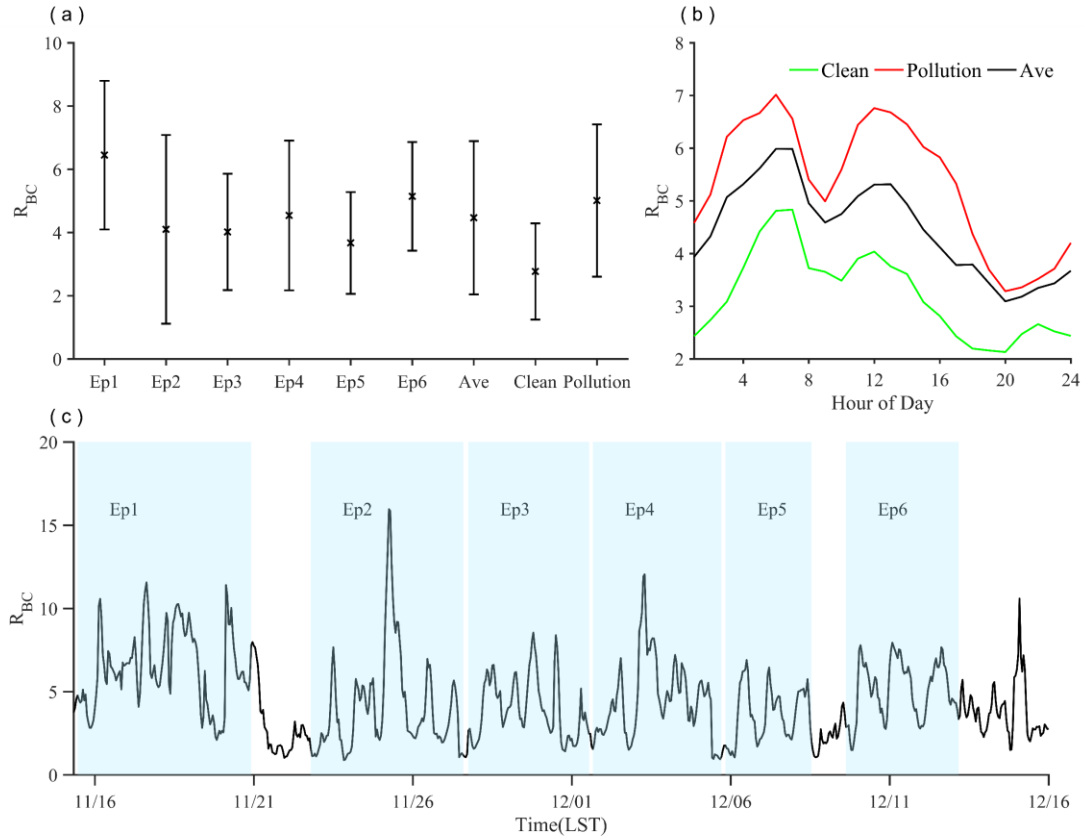

Figure 11. (a) average and standard variation of massing ratio of coating to BC (R_{BC}) during different episodes and pollution levels, (b) diurnal cycles of R_{BC} under different pollution levels, (c) temporal variation of R_{BC} during study period.

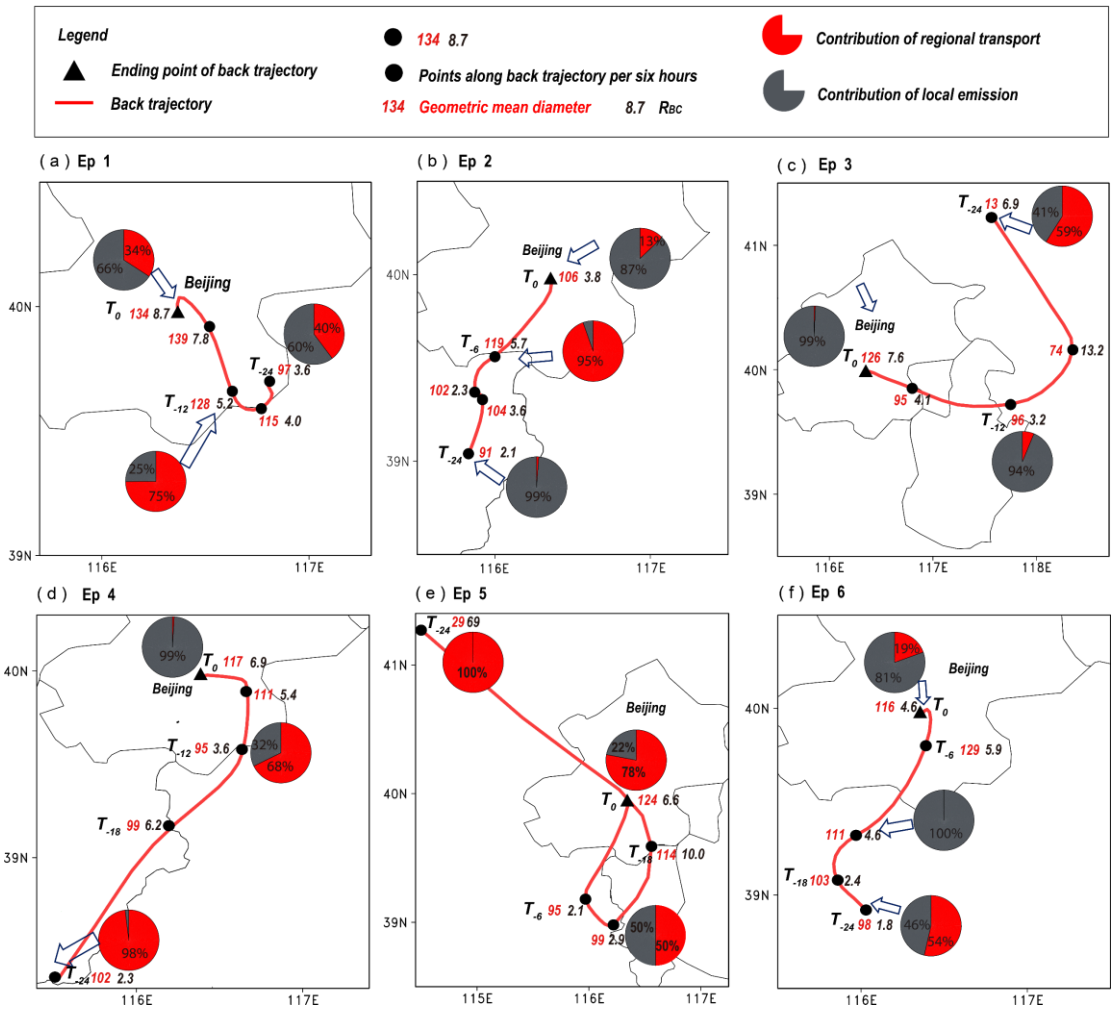

Figure 12. Variation of aerosol properties along transport. Panel a–f refers to episode 1–6. The red lines refer to 24 h backward trajectories at the altitude of 100 m. Aerosol properties include geometric mean diameter (GMD [nm], red numbers beside the solid blocks), mass ratio of coating to BC (R_{BC}, the black numbers beside the solid blocks, an indicator of aging degree), region source of BC (pies, the red represents regional transport and the gray is the local contribution). Solid black triangles are ending points of back trajectories, called T_0. Solid black circles are points along trajectories per six hours. T_{-6}, T_{-12}, T_{-18}, T_{-24} mean 6, 12, 18, 24 hours before arriving at ending site. Ending times of backtrajectories are before pollution peaks at 21:00 on November 18, 22:00 on November 25, 16:00 on November 29, 22:00 on December 03, 0:00 on December 8 and 22:00 on December 11 (LST), respectively.

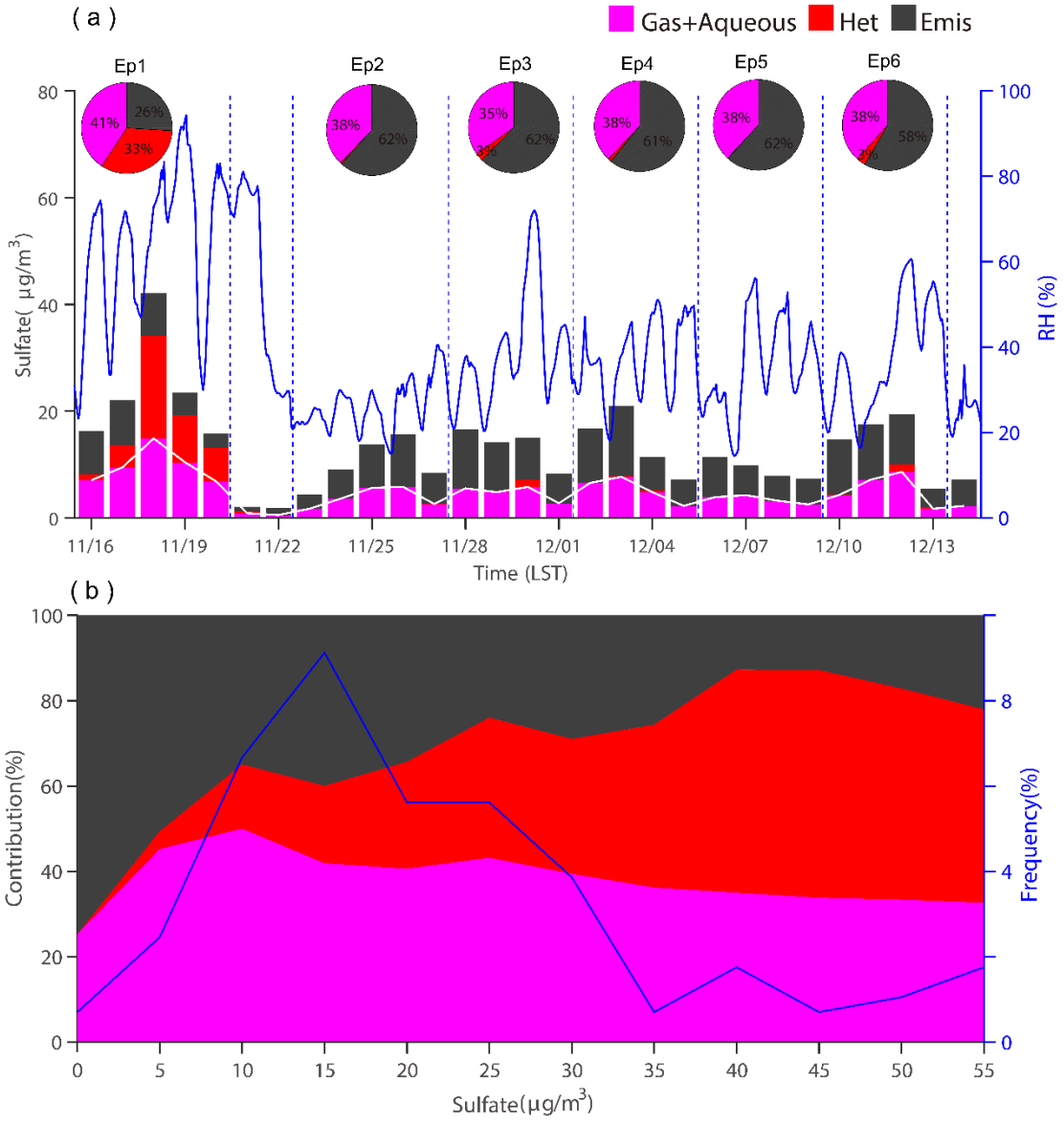

Figure 13. Contribution of different formation ways to sulfate in Beijing. (a) Daily average. Blue line shows relative humidity at Beijing. Pies show average contribution of different ways during each episode. (b) Relationship between sulphate concentration and different formation pathways of sulphate during Ep1.

Tables

Table 1. Source-tagging regions and primary $PM_{2.5}$ emissions during 15 November–15 December, 2016 in this study. [a]

Regions	Descriptions	Area 10^3 km^2	Population 10^6	GDP [b] (10^{12} CNY)	Emission [c] (10^9g)
BJ	Beijing	16.4	21.7	2.5	3.6
TJ	Tianjin	11.9	15.6	1.8	3.9

	NHB	Chengde, Zhangjiakou and Qinhuangdao	84.1	11.6	0.4	3.6
BTH	WHB	Baoding and Shijiazhuang	38.0	21.2	0.9	8.1
	EHB	Tangshan, Langfang and Cangzhou	33.9	20.3	1.1	10.1
	SHB	Hengshui, Xingtai and Handan	33.3	22.9	0.7	6.8
HN		Henan	167.0	95.3	4.0	26.6
SD		Shandong	155.8	99.5	6.8	38.5
SX		Shanxi	156.7	36.8	1.3	25.9
OT		Other regions				

[a] Regions are shown in Fig. 1c.

[b] GDP unit in 2016 is Chinese Yuan (CNY) (http://www.tjcn.org/tjgb/).

[c] $PM_{2.5}$ emissions data are obtained from the 2016 Multi–resolution Emission Inventory for China (MEIC) with 0.25° × 0.25° resolution.